



**UNIVERSIDAD DE INVESTIGACIÓN DE TECNOLOGÍA  
EXPERIMENTAL YACHAY**

**Escuela de Ciencias de la Tierra, Energía y Ambiente**

**TÍTULO: Seismic body-wave attenuation of the crust and upper  
mantle beneath Alaska**

Trabajo de integración curricular presentado como requisito para la  
obtención del título de  
Geólogo

**Autor:**

Salas Pazmiño Cristhian Paul

**Tutor:**

PhD. Foster Anna Elizabeth

Urququí, marzo de 2020

**SECRETARÍA GENERAL**  
**(Vicerrectorado Académico/Cancillería)**  
**ESCUELA DE CIENCIAS DE LA TIERRA, ENERGÍA Y AMBIENTE**  
**CARRERA DE GEOLOGÍA**  
**ACTA DE DEFENSA No. UITEY-GEO-2020-00002-AD**

En la ciudad de San Miguel de Urcuquí, Provincia de Imbabura, a los 26 días del mes de febrero de 2020, a las 11:00 horas, en el AulaCHA-01 de la Universidad de Investigación de Tecnología Experimental Yachay y ante el Tribunal Calificador, integrado por los docentes:

<b>Presidente Tribunal de Defensa</b>	Dra. PIISPA ELISA JOHANNA Ph.D.
<b>Miembro No Tutor</b>	Dr. GONZALEZ ALMEIDA RAFAEL VLADIMIR Ph.D.
<b>Tutor</b>	Dra. FOSTER ANNA ELIZABETH Ph.D.

Se presenta el(la) señor(ita) estudiante **SALAS PAZMIÑO, CRISTHIAN PAUL**, con cédula de identidad No. **172301807**, de la **ESCUELA DE CIENCIAS DE LA TIERRA, ENERGÍA Y AMBIENTE**, de la Carrera de **GEOLOGÍA**, aprobada por el Consejo de Educación Superior (CES), mediante Resolución **RPC-SE-10-No.031-2016**, con el objeto de rendir la sustentación de su trabajo de titulación denominado: **SEISMIC BODY-WAVE ATTENUATION OF THE CRUST AND UPPER MANTLE BENEATH ALASKA**, previa a la obtención del título de **GEÓLOGO/A**.

El citado trabajo de titulación, fue debidamente aprobado por el(los) docente(s):

**Tutor** Dra. PIISPA ELISA JOHANNA Ph.D.

Y recibió las observaciones de los otros miembros del Tribunal Calificador, las mismas que han sido incorporadas por el(la) estudiante.

Previamente cumplidos los requisitos legales y reglamentarios, el Tribunal, de conformidad a lo establecido en el artículo 20 del reglamento de Titulación de Grado de la Universidad de Investigación de Tecnología Experimental Yachay, que en la parte pertinente señala: "(...) Este Tribunal podrá receptor la defensa oral del trabajo final de titulación por parte de él o los estudiantes, o remitirse solamente al documento electrónico presentado de conformidad con el criterio del mismo tribunal, (...)". Revisado el documento electrónico que contiene el trabajo de titulación, por los miembros del Tribunal, deciden que no es necesario que se recepte la defensa oral del mismo, y obtiene las siguientes calificaciones:

<b>Tipo</b>	<b>Docente</b>	<b>Calificación</b>
Presidente Tribunal De Defensa	Dra. PIISPA ELISA JOHANNA Ph.D.	10,0
Miembro Tribunal De Defensa	Dr. GONZALEZ ALMEIDA RAFAEL VLADIMIR Ph.D.	10,0
Tutor	Dra. FOSTER ANNA ELIZABETH Ph.D.	10,0

Lo que da un promedio de: **10.0 (diez)**, sobre 10 (diez), equivalente a: **APROBADO**

Para constancia de lo actuado, firman los miembros del Tribunal Calificador y el/lasecretario ad-hoc.



Dra. PIISPA ELISA JOHANNA Ph.D.  
**Presidente Tribunal de Defensa**

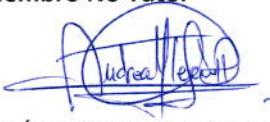


Dra. FOSTER ANNA ELIZABETH Ph.D.  
**Tutor**



Dr. GONZALEZ ALMEIDA RAFAEL VLADIMIR Ph.D.

**Miembro No Tutor**



TERÁN ROSALES, ANDREA YOLANDA

**Secretario Ad-hoc**

## AUTORÍA

Yo, **Cristhian Paul Salas Pazmiño**, con cédula de identidad 1723018097, declaro que las ideas, juicios, valoraciones, interpretaciones, consultas bibliográficas, definiciones y conceptualizaciones expuestas en el presente trabajo; así como, los procedimientos y herramientas utilizadas en la investigación, son de absoluta responsabilidad de el/la autora (a) del trabajo de integración curricular. Así mismo, me acojo a los reglamentos internos de la Universidad de Investigación de Tecnología Experimental Yachay.

Urcuquí, marzo de 2020.



---

Cristhian Salas  
1723018097

## AUTORIZACIÓN DE PUBLICACIÓN

Yo, **Cristhian Paul Salas Pazmiño**, con cédula de identidad 1723018097, cedo a la Universidad de Tecnología Experimental Yachay, los derechos de publicación de la presente obra, sin que deba haber un reconocimiento económico por este concepto. Declaro además que el texto del presente trabajo de titulación no podrá ser cedido a ninguna empresa editorial para su publicación u otros fines, sin contar previamente con la autorización escrita de la Universidad.

Asimismo, autorizo a la Universidad que realice la digitalización y publicación de este trabajo de integración curricular en el repositorio virtual, de conformidad a lo dispuesto en el Art. 144 de la Ley Orgánica de Educación Superior

Urcuquí, marzo de 2020.



---

Cristhian Salas  
1723018097

## ACKNOWLEDGEMENTS

I would first like to thank my thesis advisor Anna Foster. She was always available whenever I ran into a trouble spot or had a question about my research or writing. Anytime, she was ready to help. She consistently allowed this paper to be my own work but steered me in the right direction whenever she thought I needed it.

I would like to specially recognize to my ‘unofficial’ thesis co-advisor Zach Eilon. He gave me the opportunity to travel to United States and work on this project. He helped me a lot to develop this project. I learned a lot from him during my short stay at UCSB. I want to say thank you for being such a great person and for your unconditional help.

I also want to say thank you to all the professors that helped in my academic formation, since I started my career, here in Yachay. Specially to Elisa Piispa, she has been a fundamental person in my training as a professional and as a person.

Finally, I must express my very profound gratitude to my family and girlfriend for providing me with unfailing support and continuous encouragement throughout my years of study and through the process of researching and writing this thesis. This accomplishment would not have been possible without them. Thank you very much.

## RESUMEN

Alaska es uno de los lugares con mayor actividad sísmica del mundo y alberga una gran zona de subducción. La escasez histórica de cobertura sismológica de banda ancha nos ha dejado con muchas preguntas sin respuesta respecto a la estructura litológica y las variaciones de temperatura lateral del subsuelo de nuestro planeta. Podemos estudiar estas propiedades usando medidas de atenuación y velocidad de ondas sísmicas. Es la primera vez que los datos de este arreglo sísmico transportable desplegado en Alaska y el oeste de Canadá (AKTA) se utilizan para producir mapas de atenuación diferencial. Miles de ondas sísmicas de 857 terremotos telesísmicos registrados en el AKTA se obtuvieron de IRIS DMC. Después de seleccionar manualmente las llegadas de ondas P, S y SKS, se utilizó un método de correlación cruzada para calcular el tiempo de viaje diferencial ( $\delta t$ ), y se utilizó un enfoque de relación espectral para calcular la atenuación diferencial ( $\Delta t^*$ ). Los valores promedio para cada estación se obtuvieron utilizando un método de mínimos cuadrados, que toma en cuenta los términos de cada evento. Los mapas  $\delta t$  y  $\Delta t^*$  muestran patrones similares: en general, observamos llegadas tempranas y baja atenuación en el arco de isla Aleutiana y llegadas tardías y alta atenuación en la mayor parte de Alaska continental y el oeste de Canadá. En el caso de las llegadas S y SKS, observamos una zona con llegadas anticipadas en el noroeste de Alaska, pero este patrón no está claro en los mapas de atenuación. Estas variaciones se pueden interpretar en términos de la subducción de la placa del Pacífico debajo de la placa de América del Norte: la placa más fría exhibe velocidades mayores y atenuación reducida. Estos mapas proporcionan un marco importante para revelar las estructuras geofísicas a gran escala de esta área, pero estos resultados promedian los valores a través de la heterogeneidad tridimensional interna. Además, estos resultados se pueden utilizar en futuros trabajos para crear modelos tomográficos de atenuación.

### Palabras clave:

Atenuación, Alaska, Velocidad sísmica, Ondas de cuerpo, Zona de subducción

## ABSTRACT

Alaska is one of the most seismically active places in the world and hosts a large subduction boundary. The historical dearth of broadband seismological coverage has left us with many unanswered questions regarding the lithologic structure and lateral temperature variations of Earth's subsurface. We can study these properties using measurements of seismic wave attenuation and velocity. This study is the first time that data from the Transportable Array deployed in Alaska and western Canada (AKTA) are used to produce differential attenuation maps. Thousands of waveforms from 857 teleseismic earthquakes recorded on the AKTA were obtained from the IRIS DMC. After hand-picking P, S and SKS wave arrivals, a cross-correlation method was used in order to calculate the differential travel time ( $\delta t$ ), and a spectral ratio approach was used to calculate differential attenuation ( $\Delta t^*$ ). The average values for each station were obtained using a least-squares method, accounting for event terms.  $\delta t$  and  $\Delta t^*$  maps show similar patterns: in general, we observe early arrivals and low attenuation on the Aleutian island arc and late arrivals and high attenuation in most of continental Alaska and western Canada. In the case of the S and SKS arrivals, we observe a zone with early arrivals in northwestern Alaska, but this pattern is not clear in the attenuation maps. These variations can be interpreted in terms of the subduction of the Pacific plate beneath the North American Plate: the colder slab exhibits increased velocities and reduced attenuation. These maps provide an important framework for revealing the large-scale geophysical structures of this area, but these results average the values across internal 3-D heterogeneity. Moreover, these results can be used in future work to create tomographic models of attenuation.

### Key words:

Attenuation, Alaska, Seismic velocity, Body-waves, Subduction zone

# Table of Contents

<b>ACKNOWLEDGEMENTS</b> .....	i
<b>RESUMEN</b> .....	ii
<b>ABSTRACT</b> .....	iii
<b>1. Introduction</b> .....	1
1.1 Local structure, scattering, and multipathing.....	1
1.2 Instrument response.....	2
1.3 Geometrical spreading .....	2
1.4 Intrinsic attenuation .....	2
1.5 Attenuation studies .....	3
1.6 Previous attenuation and velocity studies in Alaska.....	4
1.7 AKTA.....	6
<b>2. Tectonic setting</b> .....	7
2.1 Aleutian subduction zone.....	8
2.2 The Yakutat Plateau.....	8
2.3 Regional geology .....	9
2.4 Earthquake Distribution.....	9
<b>3. Alaska: Motivation and objectives</b> .....	11
<b>4. Methodology</b> .....	12
4.1 Data collection.....	12
4.2 Pre-processing.....	12
4.3 Differential travel time ( $\delta t$ ).....	14
4.4 Differential attenuation ( $\Delta t^*$ ) .....	16

---

4.5 Smoothing.....	17
<b>5. Results.....</b>	<b>17</b>
5.1 Differential travel time ( $\delta t$ ).....	17
5.2 Differential attenuation ( $\Delta t^*$ ).....	21
<b>6. Discussion.....</b>	<b>24</b>
6.1 Tectonic interpretation.....	25
6.2 Uncertainty.....	29
<b>7. Conclusions.....</b>	<b>30</b>
<b>8. Future work and recommendations.....</b>	<b>30</b>
<b>Bibliography.....</b>	<b>32</b>
<b>Web resources.....</b>	<b>36</b>

# 1. Introduction

Amplitude and waveform shape of seismic waves contain valuable information about Earth structure and seismic source. For this reason, the study of the different factors that could affect both amplitude and waveform shape is crucial to understanding Earth's interior and the processes that are occurring underground. Wave amplitude can be affected by different frequency-dependent processes, such as scattering, multipathing, local structure, instrument response, and intrinsic attenuation. Most of them are elastic processes except intrinsic attenuation, local structure and instrument response. Wave amplitudes can also be affected by the frequency-independent factor called geometrical spreading; this process is an elastic contribution as well [Cafferky and Schmandt, 2015; Eilon and Abers, 2017; Shearer, 2009]. In this study, we will focus on the frequency-dependent factors that decrease the amplitude of seismic waves, specifically anelastic attenuation. In this section many of the important concepts will be introduced in order to understand this study.

## 1.1 Local structure, scattering, and multipathing

The local structure is an important factor to consider because depending of the tectonic setting of the study area, it is possible to observe different patterns. For instance, the tectonically inactive region of the eastern USA shows low values of attenuation while the active margin of the western USA shows high values of attenuation [Cafferky and Schmandt, 2015]; in a midocean ridge (MOR) we expect to have a more homogeneous distribution of high values of attenuation caused by melting effects [Eilon and Abers, 2017]. In a subduction zone it is typical to find low values of attenuation for the cold slab that is being subducted and high values of attenuation in the back-arc basins [Roth et al., 1999].

Scattering is a process that occurs when the energy of a wavefield is scattered into different phases because of the changes in material properties, particularly at sharp boundaries, but the integrated energy in the total wavefield remains constant. Depending on the material properties, this can lead to amplitude decay and dispersive effects.

Finally, multipathing is a consequence of lateral velocity variations. Seismic waves refract toward low-velocity anomalies and away from high-velocity anomalies. Seismic waves will not travel in the predicted ray path and this can affect our measurements [Stein and Wyssession, 2009].

## 1.2 Instrument response

Seismic instruments record electric pulses created by ground motion, but the amplitude of the signal will depend on different factors, including the brand of the instruments, the instrument's natural frequency, and several installation factors. It is needed to recover the ground displacement from a given recorded signal, which is done by applying a correction for the instrument response [Havskov and Alguacil, 2004]. This correction allows to standardize the signals between different deployed seismometers to carry out this study.

## 1.3 Geometrical spreading

Geometric spreading is the change in amplitude of a wave as the energy of a spherical wave front emanating from a point source is distributed over a spherical surface of ever-increasing size, [Margerin and Sato, 2011; Shearer, 2009]. Propagation of seismic waves will decrease the energy per unit area and consequently the amplitude of those waves will decrease as waves travel away from the source.

## 1.4 Intrinsic attenuation

Intrinsic attenuation (or anelastic attenuation) refers to the conversion of seismic energy to heat by permanent deformation of the medium. It also causes a reduction in the amplitude of a wave with increasing distance traveled. The strength of intrinsic attenuation is given by the factor  $Q$ , a dimensionless quantity that describes the fractional energy loss per cycle:

$$Q = 2\pi \frac{E}{\Delta E}, \quad (1)$$

where  $E$  is the peak of strain energy and  $\Delta E$  is the energy loss per cycle.  $Q$  is also referred to as the quality factor and is inversely related to amplitude loss [Shearer, 2009]. Intrinsic attenuation observations are crucial to investigate Earth's interior: these observations provide a valuable source of information about the thermal properties and composition of the subsurface at different depths [Piccinini et al., 2010]. The proper interpretation of seismic wave attenuation provides insight into where temperatures and water content may allow melting to take place and can provide important clues to Earth's thermochemical and stress state [Karato and Spetzler, 1990; Stachnik et al., 2004]. The main factors that control  $Q$  are related to grain size, water and melt content and all of them are linked [Eilon and Abers, 2017].

## 1.5 Attenuation studies

There are different global models of seismic attenuation that provide important insight into the thermal structure of the interior of the planet, especially in the upper mantle [e.g., Dalton et al., 2008; Gung and Romanowicz, 2004; Reid et al., 2001, Romanowicz, 1995; Selby and Woodhouse, 2002]. These models are useful because they provide context for the results of more local studies. In general, comparisons with other models help to identify systematic similarities and the reasons for significant discrepancies [Dalton et al., 2008]. Global models show that spreading ridges are areas of high attenuation and these high values are interpreted as a result of high temperatures. The active margin of the western coast of North America is also a region of high attenuation; indeed, in general, active margins are regions of high attenuation. In contrast, areas of low attenuation are located beneath stable continental interiors without any recent tectonic activity, as well as passive margins [Dalton and Ekström, 2006; Dalton et al., 2008].

Seismic attenuation models can be produced using either body or surface seismic waves. In order to develop them, it is required to have a large data set of Rayleigh or P and S wave amplitudes collected by a dense network. Then, the spectra of these amplitudes are inverted for the different coefficients of the model [Dalton et al., 2008]. Surface wave studies provide

good vertical resolution but not lateral. In this study, we will use body waves because they better allow us to obtain lateral resolution than surface waves [Eilon and Abers, 2017].

Using the same principles, we can bring this kind of study to the regional and local level. Local studies may target a specific structure, for instance a volcano or a fault [e.g., Bianco et al., 1999; Gudmundsson et al., 2004]. Regional studies, such as Cafferky and Schmandt (2015), who created a seismic P-wave attenuation map of the contiguous USA, often take advantage of new, high quality data sets like the USArray Transportable Array (TA). In this study, we will produce similar results for Alaska by using the data set from Transportable Array deployed in Alaska and Western Canada (AKTA).

## 1.6 Previous attenuation and velocity studies in Alaska

In 2004, Stachnik et al. came up with a model of seismic attenuation for central Alaska and a new model of the mantle thermal structure. They used data from the Broadband Experiment Across the Alaska Range (BEAAR) that was the first dense broadband seismic deployment in Alaska, covering an area of about 150 km<sup>2</sup>. The Q structure was imaged beneath central Alaska at high resolution, and they found that this subduction zone has a pattern similar to other subduction zones. However, the highest values of attenuation were low compared to other subduction zones. This was interpreted in terms of a cold mantle wedge that has lower temperatures compared with mantle wedges in other subduction zones [Stachnik et al., 2004]. This study related the absence of arc volcanism in the Denali volcanic gap to the low values of attenuation. However, because of the limited extent of this array it was not possible to assume that the values of attenuation would be the same along the different sections of the subduction zone. Additionally, with the data and station spacing available in their study, within the mantle wedge the value of uncertainty was about 10% of the real value for both P and S waves. The data from AKTA that will be used in our study will cover a bigger area and we will be able to provide more information about Alaska with lower uncertainty.

Velocity models provide a useful comparison with attenuation studies because both types of data are sensitive to the same Earth structure. The global models of seismic attenuation show a strong anticorrelation with seismic velocity models, which means areas with low velocities typically have high attenuation. In addition, the sensitivity of attenuation to factors such as temperature, composition, partial melt, and water content is different from that of seismic velocity [Dalton and Ekström, 2006]. Anelastic effects have a stronger sensitivity to temperature than seismic velocities [Anderson and Hart, 1967; Karato and Jung, 1998]. There are many active and passive seismic source studies looking at the velocity structure of the Alaskan crust and upper mantle [e.g., Bauer et al., 2014; Coulson et al., 2018; Jiang et al., 2018; McNamara and Pasyanos, 2002; Stachnik et al., 2004; Wang and Tape, 2014]. In 2018, Jiang and coauthors imaged the mantle shear velocity ( $V_s$ ) structure in depth beneath AKTA using a joint inversion of Rayleigh wave dispersion and teleseismic S-wave travel times (Figure 1). The two main conclusions of this study were the presence of a cold lithosphere in the north that is controlling the deformation of the southern areas, and a potential slab beneath the Wrangell volcanic field accompanied with the presence of a slab tear [Jiang et al., 2018]. We will make a comparison of the Stachnik et al. (2004) and the Jiang et al. (2018) results with the model of attenuation obtained from this thesis for our interpretation of the results.

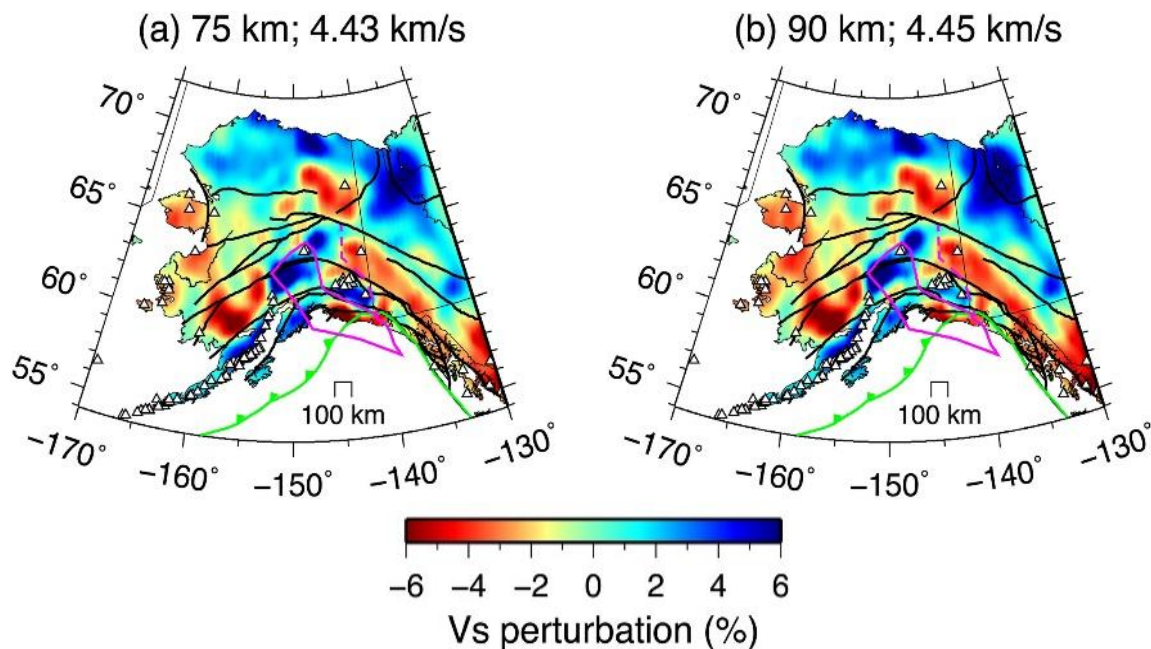


Figure 1: Depth slices through the S-velocity model at 75 and 90 Km. Modified from Jiang et al. (2018)

## 1.7 AKTA

The USArray Transportable Array is an array of broadband seismometers installed throughout the USA. After being deployed in the contiguous United States between 2007-2014, the instruments were moved north, to Alaska and western Canada. Between 2011 and 2013 some test stations were installed before deployment began in 2014. This array is called the ‘Transportable Array deployment to Alaska and Western Canada’ and we will refer to it here as AKTA (Figure 2). It comprises 285 stations that will continue collecting data until 2020. The array includes 88 cooperating stations from existing networks operated by the Alaska Regional Network, National Tsunami Warning System, Alaska Volcano Observatory, Canadian National Seismograph Network, Global Seismograph Network (GSN - IRIS/IDA), Global Seismograph Network (GSN - IRIS/USGS), Yukon Northwest Seismic Network (YNSN), United States National Seismic Network and the Yukon Observatory. This array is a grid of stations spaced about 85 km apart covering all of mainland Alaska and parts of the Yukon, British Columbia, and the Northwest Territories in Canada. In addition, all the data obtained by the equipment of this array is publicly available and can be accessed via the Data Management Center of the International Research Institutes for Seismology (IRIS DMC) [Fee et al., 2017; Jiang et al., 2018; USArray.org].

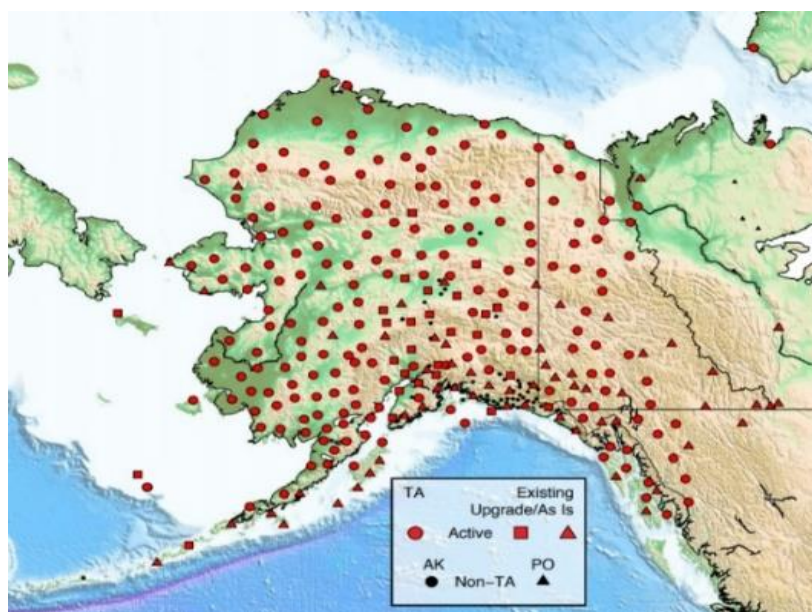


Figure 2. AKTA array. Modified from USArray.org

## 2. Tectonic setting

Alaska is located on the Ring of Fire, a zone around the Pacific Ocean with high volcanic and seismic activity. In the specific area of Alaska, two main tectonic processes are happening. The first process is the subduction of the Pacific Plate beneath the North American Plate. This subduction yields large earthquakes and volcanism in this area. The second process has to do with the collision and accretion of the thicker Yakutat Plateau located atop the Pacific Plate [Bruns, 1983; Christeson et al., 2010; IRIS.edu]. In this section, we will describe these two processes and some other important aspects related to the tectonic setting of our study area.

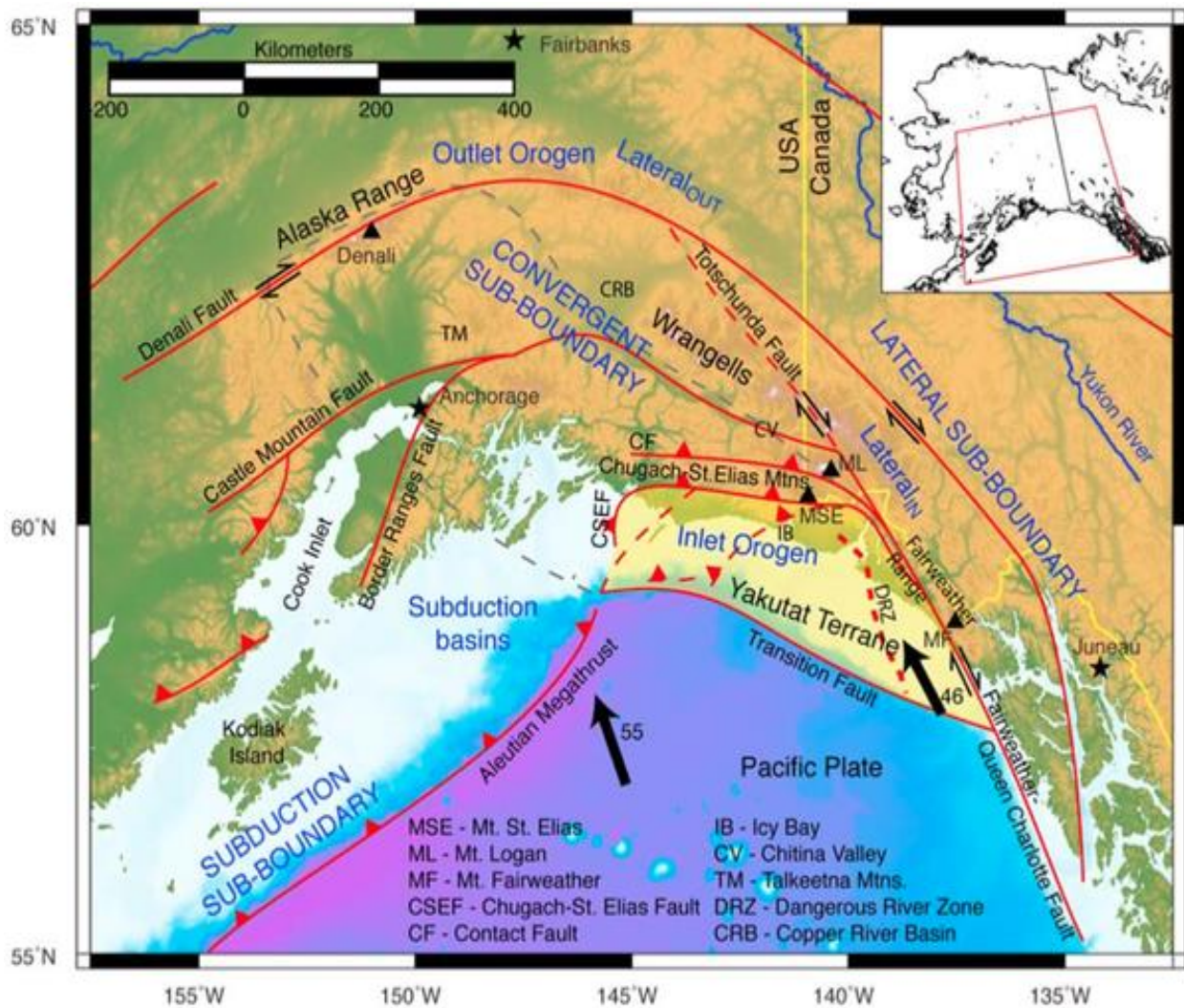


Figure 3: Tectonic setting of Alaska. Modified from Koons et al. (2010)

## 2.1 Aleutian subduction zone

In this area the oceanic Pacific Plate is subducting beneath the continental North American Plate. The oldest section of the Pacific plate is early Cretaceous, approximately 145 Ma. Its average thickness is about 100 km. The most distinctive features of this plate are the Hawaiian hot spot, and a seamount chain close to the Gulf of Alaska. The current subduction process started in the early Eocene, about 55 Ma ago [Brown et al., 2013]. The Kula plate was subducted prior to the subduction of the Pacific plate. The spreading process between both plates ceased due to subduction of their spreading ridge beneath the Aleutian island arc [Byrne, 1979]. This subduction zone presents important lateral variations regarding different aspects. On the eastern end, close to the Gulf of Alaska, the Pacific Plate is subducting at a rate of 5.5 cm/yr (Figure 3). At this side of the subduction zone, the angle of subduction is shallow and the section of the Pacific Plate that is being subducted is about ~20 Ma. On the western end, close to the Near Islands, subduction occurs at a rate of 7.8 cm/yr. At this side, the angle of subduction is steeper than on the eastern side and the downgoing plate is older, about ~70 Ma [Christeson et al., 2010; Scholl et al., 1987; Holbrook, 1999]. The distance between the trench and the volcanic arc is about 170 km on the western end and 360km on the eastern end [IRIS.edu].

## 2.2 The Yakutat Plateau

The Yakutat Plateau is a thick fragment of oceanic crust that was formed about 50 Ma [Christenson et al., 2010]. This zone shows differences in velocity and thickness compared to the Pacific Plate. This block is thicker, about 30km, and it moves at a rate of 4.4 cm/yr to the northwest relative to North America, a slower rate compared to the Pacific Plate. This difference in displacement is accommodated at the southern limit of this block by the Transition fault [Bruns, 1983]. The collision process between the Yakutat block and the North American Plate started in the Miocene and is one of the few active accretion processes at present. This plateau puts more compressive pressure on the North American continental plate causing the formation of the Chugach-St. Elias orogeny, beginning about 6 Ma ago,

and causes broad deformation throughout southern Alaska, as well. Volcanism is not present in this specific area [Christeson et al., 2010; Ferris et al., 2003; IRIS.edu; Jiang et al., 2018].

## 2.3 Regional geology

The geology of Alaska is very complex. Its territory is composed of many accreted terrains that are separated by mostly active faults. Some of the most important are the Tintina, Denali, Contact, Border Ranges, Transition, and Queen Charlotte faults (Figure 4). These main faults are separating different terranes, among them the North American Craton, Yakutat terrane, Prince William terrane, Peninsular terrane, Chugach terrane, Wrangellia terrane, and Yukon composite terrane. This zone also contains different old volcanic arcs and mountain ranges such as the Brooks Range, Richardson Mountain, Mackenzie Mountain, Alaska Range, and St. Elias Range [Jiang et al., 2018]. In general, Paleozoic and Mesozoic sedimentary rocks are the most common rock units through Alaska. There is also an important concentration of igneous rocks, both intrusive and volcanic, in most mountain ranges from the Precambrian to the Cenozoic [Beikman, 1980]. The Aleutian subduction zone has an important number of volcanoes along the arc, but there are two main areas that need to be highlighted: the first is the Denali volcanic gap, where there are no volcanoes; the second is the Wrangell Volcanic field that in contrast has a higher concentration of volcanic activity. These anomalous regions are explained in terms of low mantle wedge temperatures and fragmentation or tearing of the slab, respectively [Jiang et al., 2018; Stachnik et al., 2004].

## 2.4 Earthquake Distribution

Alaska is a seismically active state: it has about 24000 earthquakes every year, and it has on average an event of  $>M_w 7$  every two years. The seismicity is concentrated close to the volcanic arc and follows the expected pattern, with shallow events that extend from near the base of the trench to depths of 40 to 60 km and the deepest events to the north within

the subducting Pacific plate, which can reach depths of 300 km (Figure 5). As expected, most of the earthquakes that occur close to the subduction zone result from thrust faulting, whereas some of the events that occur inside the North American Plate are associated with the strike-slip faults that are bounding the accreted terranes. In addition, deformation of the overriding North American plate due to Yakutat underplating generates shallow crustal earthquakes. There are also events associated with normal faulting as result of the bending of the oceanic Pacific plate as it enters the Aleutian trench [Ruppert et al., 2007, USGS].

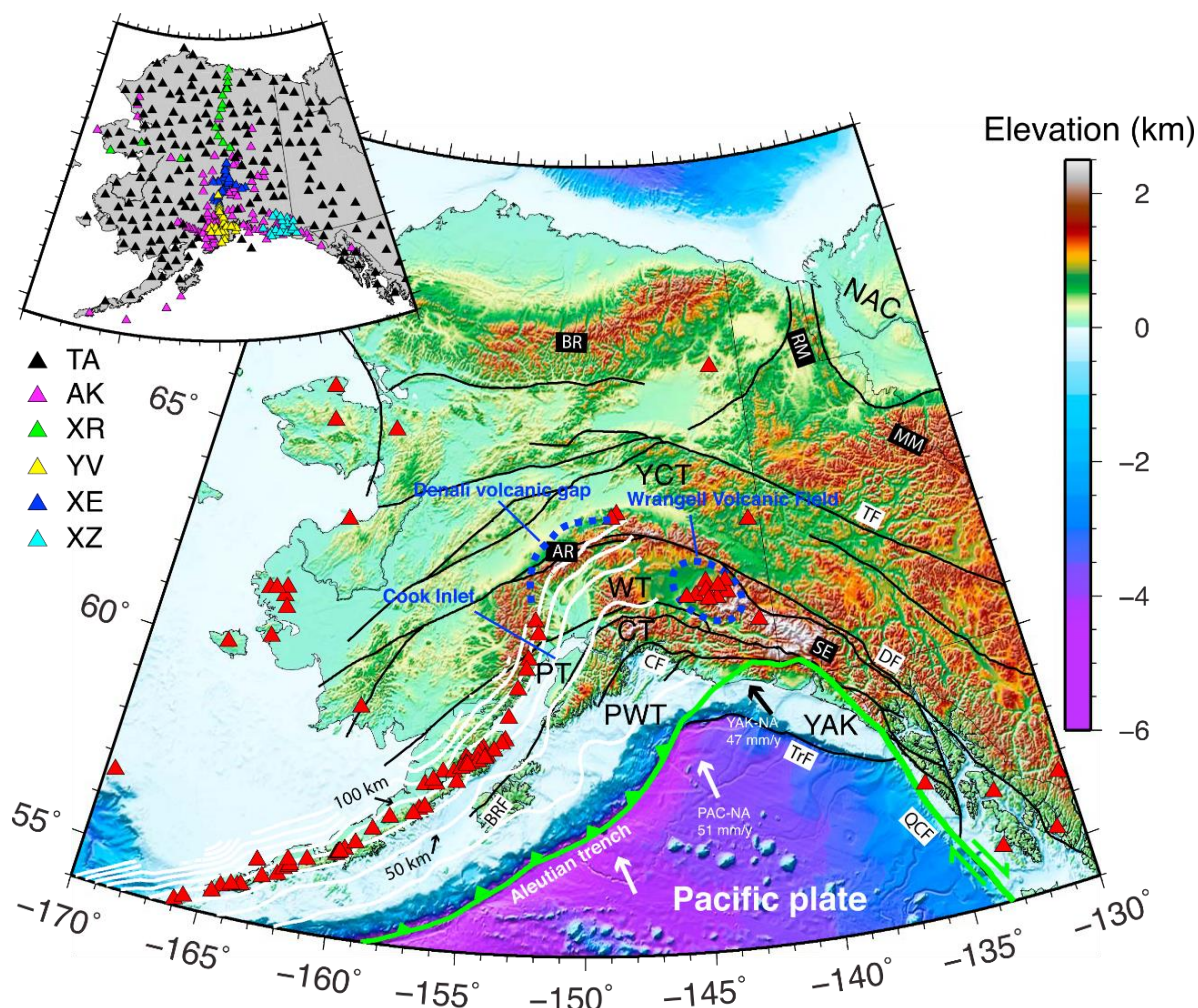


Figure 4: Elevation map with the important features of the geology of Alaska, modified from Jiang et al. (2018). Red triangles denote <2 Ma volcanoes. The green line marks the Pacific plate boundary. Black lines represent major faults including TF = Tintina fault, DF = Denali fault, CF = Contact fault, BRF = Border Ranges fault, TrF = Transition fault and QCF = Queen Charlotte fault. NAC = North American Craton, YAK = Yakutat terrane, PWT = Prince William terrane, PT = Peninsular terrane, CT = Chugach terrane, WT = Wrangellia terrane, and YCT = Yukon composite terrane. Mountain ranges are labeled as BR = Brooks Range, RM = Richardson Mountain, MM = Mackenzie Mountain, AR = Alaska Range, and SE = St Elias Range. The inset shows the AKTA.

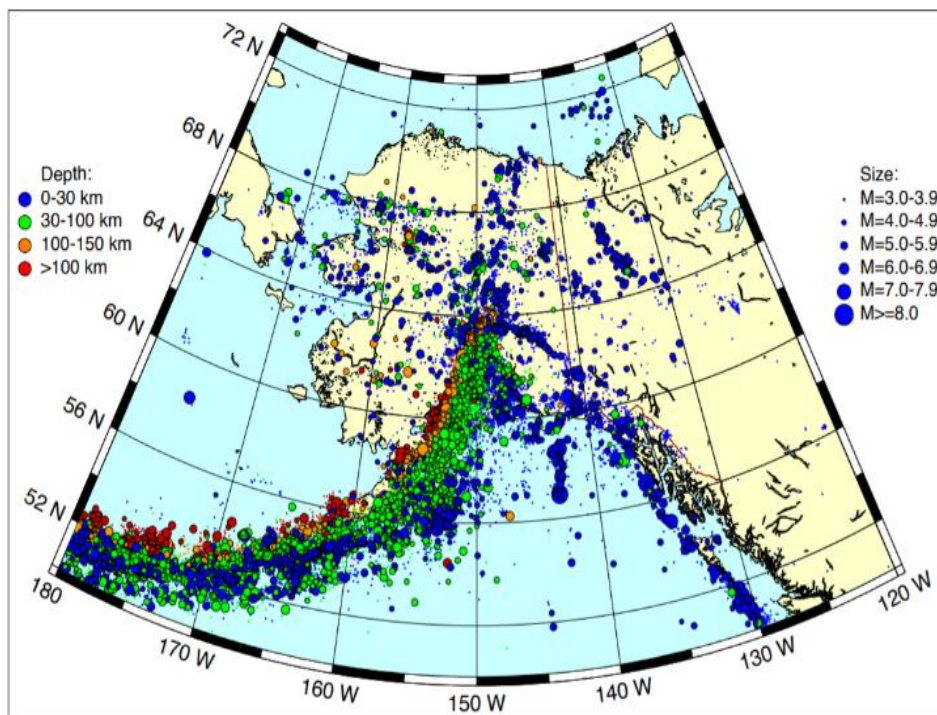


Figure 5: Earthquake distribution of Alaska between 1970-2012. Modified from USArray.org

### 3. Alaska: Motivation and objectives

There are several scientific reasons to study Alaska: it is one of the most seismically active places in the world. This place hosted the second largest instrumentally recorded earthquake worldwide: an Mw 9.2 earthquake occurred in 1964 that generated a big tsunami with waves that reached 70 meters and caused 131 deaths in total, a small number considering the magnitude of this earthquake [Alaska Earthquake Center; USGS.gov]. Alaska has more large and moderate earthquakes than the rest of the USA combined. The seismicity is varied in nature and magnitudes and spread across the whole area. The new stations of the AKTA have already greatly increased earthquake detections and data available. This is not the first array deployed in Alaska, but it is the biggest one. This incredible coverage will allow us to improve our knowledge about Earth's structure beneath Alaska and western Canada. The main objective of this study was to elucidate the attenuation and velocity patterns of Alaska since they provide crucial information about Earth's structure and the thermochemical state of the subsurface.

## 4. Methodology

The main technique used in this study is the measurement of differential attenuation between a source-receiver pair for teleseismic earthquakes. In this section, we explain the methodology used to filter and process our data set in order to obtain our attenuation and velocity maps.

### 4.1 Data collection

The data required to perform this study were obtained from the DMC of IRIS. Several constraints were used to limit the stations and the events that were selected for the measurements. We use all stations within the region bounded by the parallels  $50^\circ$  and  $73^\circ$  N and the meridians  $-180^\circ$  and  $-120^\circ$  E. This area spans the footprint of the AKTA and includes many other seismic stations from long-term regional observatories and previous temporary deployments. A total number of 1022 seismic stations were selected for this study (Figure 6). We used earthquake data from events at great-circle distances between  $20^\circ$  and  $145^\circ$  from the center of our study area,  $[64^\circ, -160^\circ]$ , and selected all events between Mw 6 and Mw 8 that occurred between January 2013 and July 2019. A total of 857 earthquakes meet these criteria (Figure 7). We obtained 30 minutes of data following each origin time for all the events at all stations, at a sample rate of 100 Hz. We downloaded the data and associated metadata using automated Matlab scripts that use IRIS DMC request tools. For the seismograms, we used an *irisFetch* request and for the seismic response files, we used a *BREQFAST* request. Additionally, we used the tool *rdseed* to read and process all the response files.

### 4.2 Pre-processing

First, the orientation of the horizontal components was corrected using the channel azimuths recorded in the metadata. The next step was to remove the seismic response of the instruments using SAC pole-zero files extracted from dataless seed files. It is important

to note that the same station can have different response files for different time periods, since any time a station's instruments are fixed or replaced, this may change the seismic response of the station. Thus, it is necessary to select the correct response file for each station during a period. For each event, we extracted data from all available stations into a single MATLAB structure for more streamlined processing. In order to window the data, we use the *TauP* Matlab toolbox. This toolbox uses 1-D velocity models to estimate the arrival time of the different seismic phases for different epicentral distances. In this study, we used the iasp-91 velocity model developed by Kennett and Engdahl (1991) to calculate the predicted arrival times for P, S, PKS, and SKS waves. We resampled the data to 5 Hz and windowed them with respect to the predicted arrival times, 200 seconds before and 100 seconds after the predicted arrival time for all the phases.

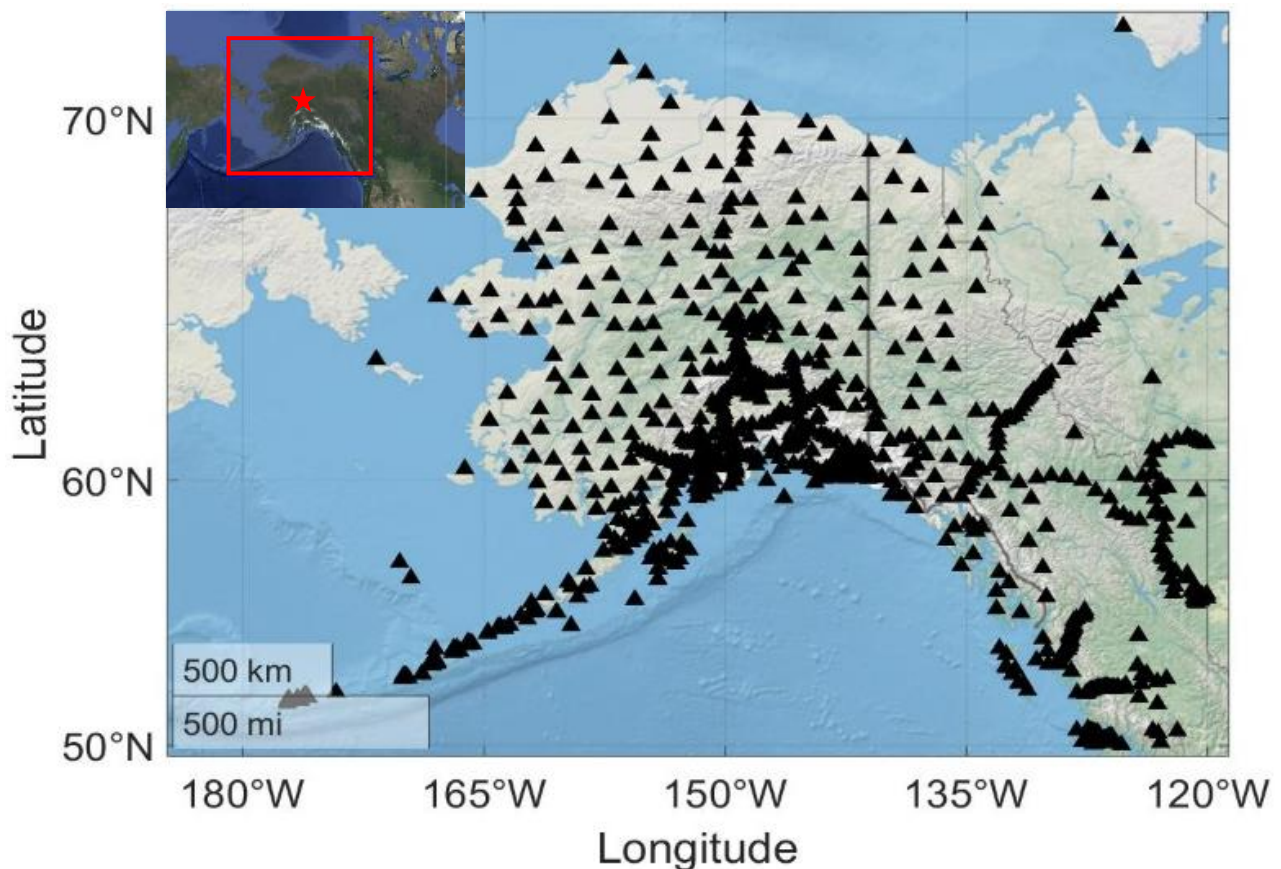


Figure 6: Seismic stations used in this study. From the seismic networks and deployments: AKTA, 1E, 5C, 5F, 7C, 7J, AK, AT, AV, CN, DE, DW, GM, II, IM, IU, NY, PN, PO, PP, SH, TA, US, XE, XF, XI, XL, XM, XN, XO, XR, XV, XY, XZ, Y2, YE, YG, YM, YO, YV, YY, ZE, ZQ. The inset is showing the studied area and the center of our array.

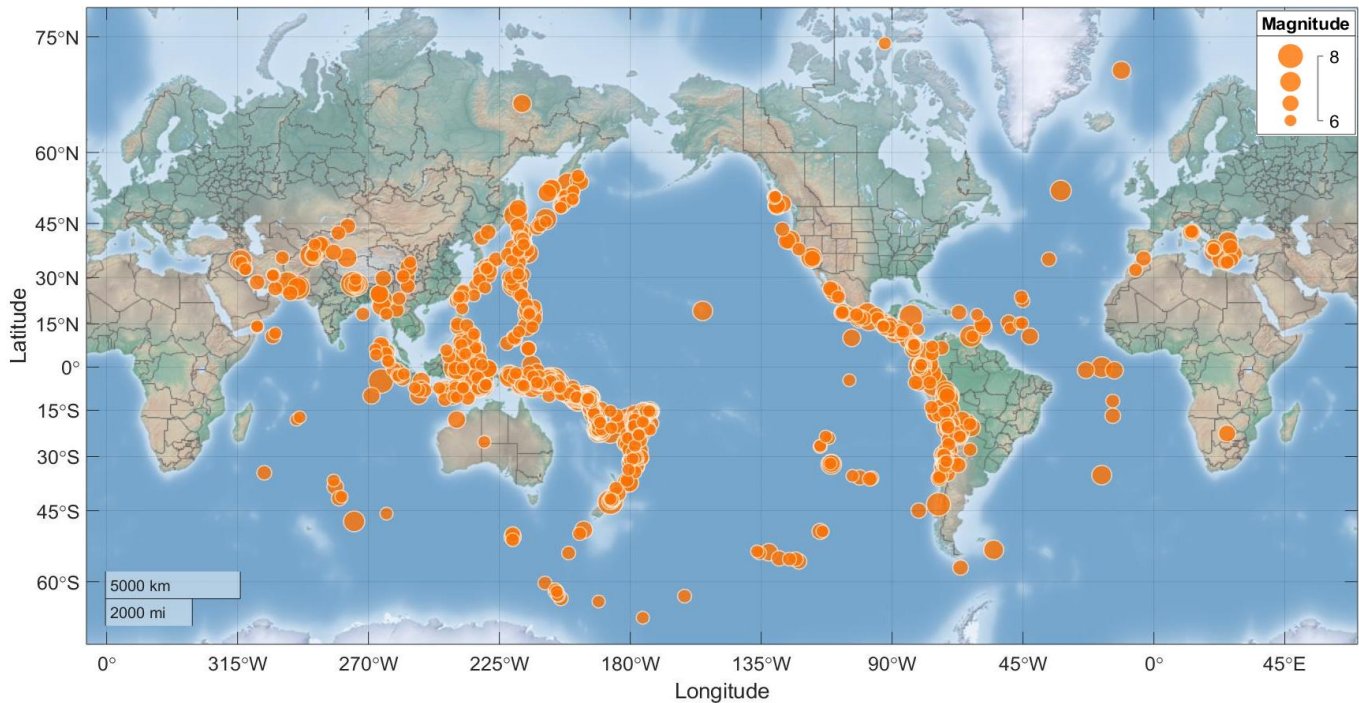


Figure 7: Teleseismic earthquakes used in this study, from the time period 2013-2019.

### 4.3 Differential travel time ( $\delta t$ )

The differential travel time is the difference in arrival times for one phase between stations. A cross-correlation method was used to measure the differential travel time across our array. In this method, we go station by station and compare the trace for the same earthquake at a single station with all other stations within a radius of  $5^\circ$ . We find the time shift needed to align the traces and a scaling factor, if required. We use a MATLAB GUI tool for this step. Within this tool, we (1) applied manual quality control to remove the remaining noisy stations, (2) defined the cross-correlation window, and finally (3) hand-selected the arrival time using a stack of all the traces (Figure 8). For the manual selection of arrivals, we considered several factors. First, we used  $TauP$  to calculate theoretical arrival times for our seismic phases. We fixed a time window around this predicted arrival, cross-correlated all the traces, and finally, we used the cross-correlated traces to pick the arrival time for each phase. We used different frequency bands and different components for each arrival. For P, we used the vertical component and a frequency band between [0.2-1] Hz. For both S and SKS, we used a frequency band between [0.04-0.125] Hz, but we used the transverse

component for S arrivals and the radial component for SKS arrivals. We examined initial measurements of PKS, but we determined that the quality and the number of measurements were not enough to include them in this study.

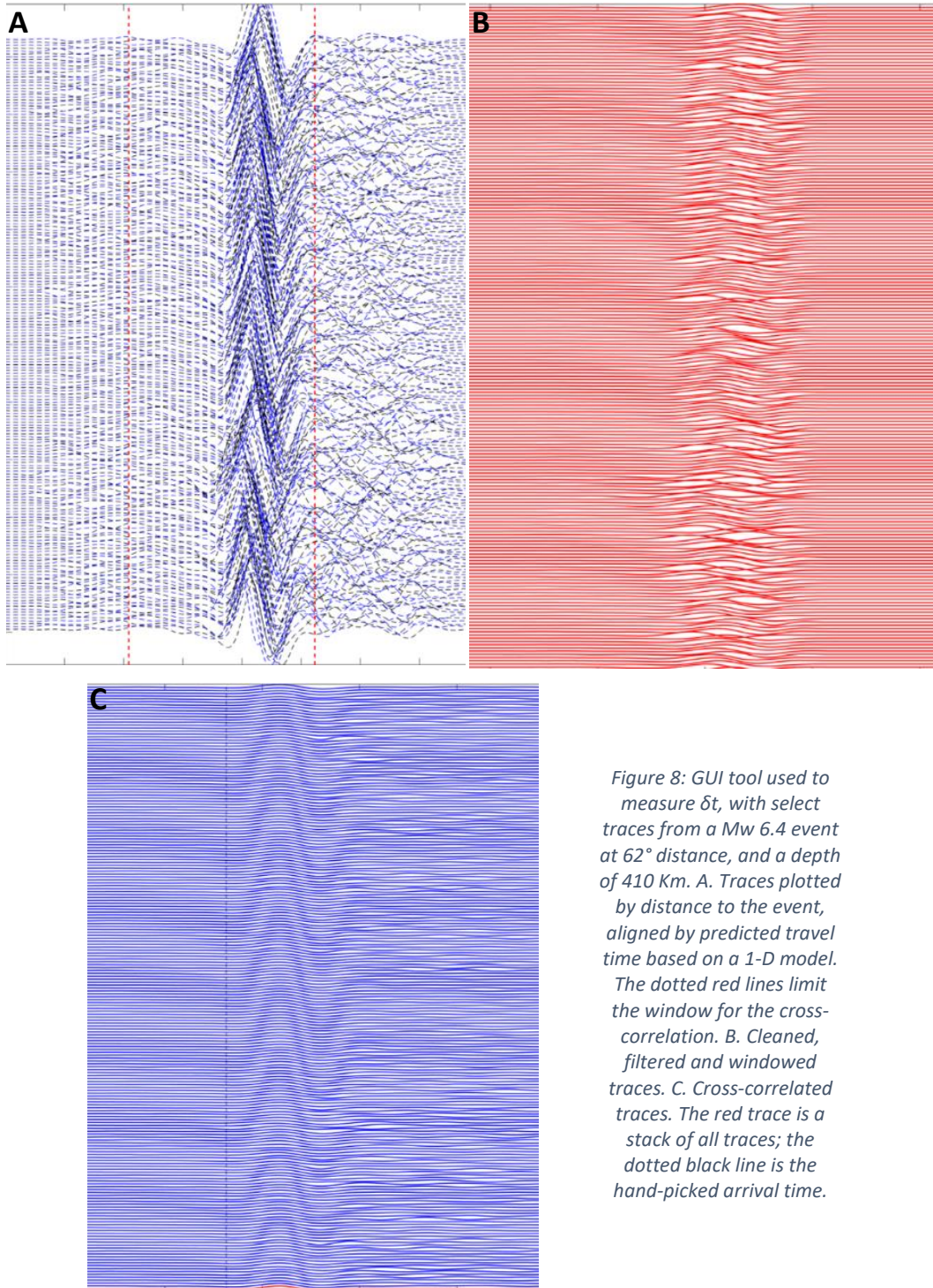


Figure 8: GUI tool used to measure  $\delta t$ , with select traces from a Mw 6.4 event at  $62^\circ$  distance, and a depth of 410 Km. A. Traces plotted by distance to the event, aligned by predicted travel time based on a 1-D model. The dotted red lines limit the window for the cross-correlation. B. Cleaned, filtered and windowed traces. C. Cross-correlated traces. The red trace is a stack of all traces; the dotted black line is the hand-picked arrival time.

## 4.4 Differential attenuation ( $\Delta t^*$ )

The parameter  $t^*$  is a non-physical body wave attenuation parameter that contains information about  $Q$  but averages across internal 3-D heterogeneity. The reason why we use it is because it simplifies the calculations. The parameter  $t^*$  contains information for both travel time and attenuation that is integrated along the ray path. It is defined as:

$$t^* = \int_R \frac{dt}{Q} \quad (2)$$

where  $dt$  is the travel time along the ray path and  $Q$  is the quality factor that measures the anelastic loss of seismic energy [Cafferky and Schmandt, 2015; Teng, 1968]. Higher values of  $Q$  indicate less attenuation and lower values, more attenuation.  $\Delta t^*$  is defined as the differential attenuation between a pair of stations for a single event.

In order to calculate differential attenuation, we used the spectral ratio approach. We computed individual station spectra using the multitaper method developed by Thomson (1982). This method provides more stable spectral estimates using short data excerpts than a simple Fourier transform does. Using this method, we estimated the amplitude spectra for a fixed window of signal and one of noise. The signal window was 5 seconds before to 15 seconds after the picked arrival time. The noise window was from 150 to 10 seconds before the picked arrival time. A comparison of the signal and noise spectra allows us to determine the frequency band at which signal amplitude is higher than noise amplitude. After obtaining the amplitude spectra, we used this information to produce measurements of attenuation. Assuming that the  $Q$  factor is frequency independent, at least in the frequency band selected, we can estimate the differential body wave attenuation parameter  $\Delta t^*$ . By using a least-squares regression of the spectral ratio of the signals, we obtained the value of  $\Delta t^*$  for each station pair that was within a radius of  $5^\circ$  with respect to the initial station [Eilon and Abers 2017]. Finally, we calculate an average station  $\Delta t^*$  for each station relative to the cumulative array by solving a least-squares problem accounting for event terms.

## 4.5 Smoothing

In order to observe and interpret the large-scale structures of Alaska, we smoothed the maps of attenuation and velocity. These smoothed maps allow us to minimize the effect of scattering that in general will have a random effect. In order to do this, we created a grid in the study area with nodes every 0.4 degrees in latitude and longitude, and at each one, we calculated a spatial average using a Gaussian function with a width of 1.5 degrees. This function weighs all our stations by distance; stations with distances greater than 250km have a weight of zero in the average.

## 5. Results

Our final results are maps for differential travel time and for differential attenuation.  $\delta t$  and  $\Delta t^*$  maps of all the arrivals show similar large-scale patterns: in general, we observe early arrivals and low attenuation on the Aleutian island arc and late arrivals and high attenuation in most of continental Alaska and western Canada. In this section we will show our results and the observations that could be made from our maps.

### 5.1 Differential travel time ( $\delta t$ )

Station averages of differential travel time ( $\delta t$ ) for P arrivals are shown in Figure 9. The observed values of  $\delta t$  range between -1.1 s and 1.1 s (Figure 13). For this map, 682 events and 423 stations were used. The minimum number of events recorded by one station was 26 and the maximum was 441. Here, it is possible to define three regions, with different patterns. First, all the stations that are on the Aleutian arc show fast arrivals represented in blue. The second region comprises southeastern Alaska and northwestern Canada: this region shows slow arrivals, represented in red. The remaining area of Alaska, mostly western Alaska in general, represents the third area. It shows fast arrivals with some stations with  $\delta t$  values between -0.1 s and 0.1 s represented in white.

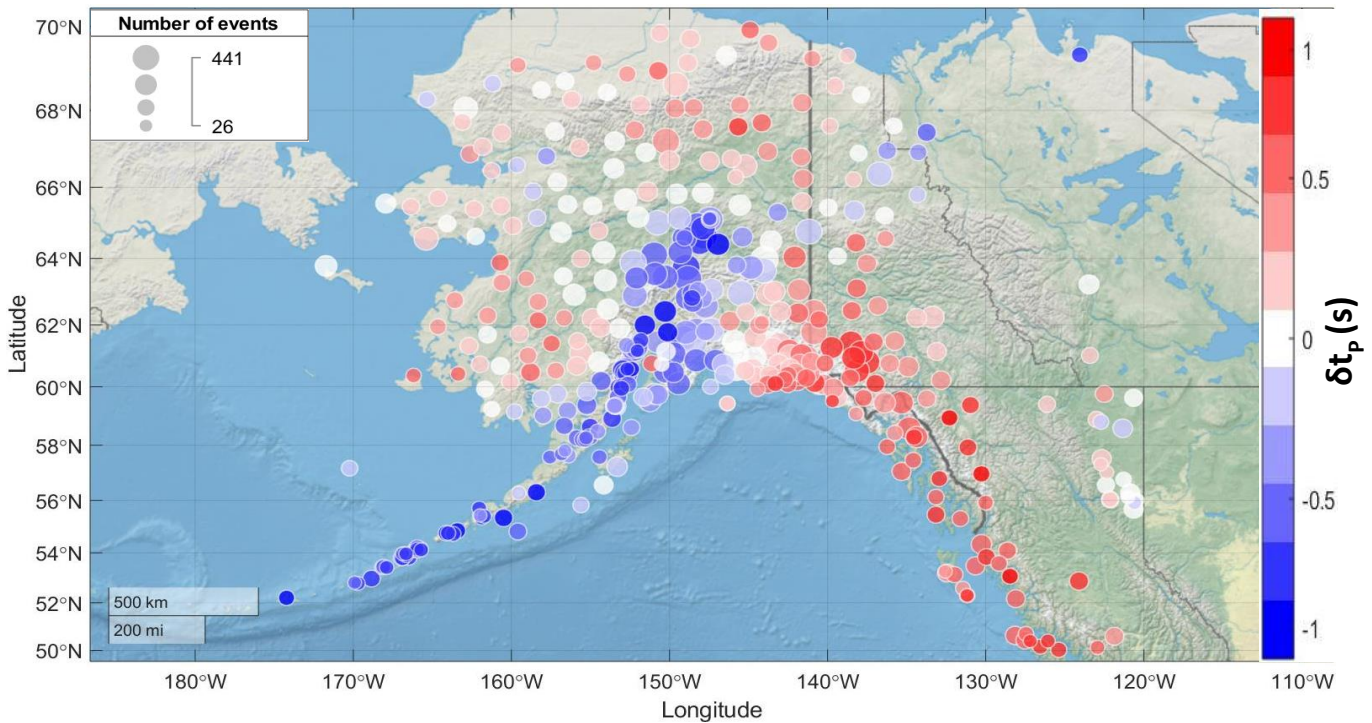


Figure 9:  $\delta t$  for P-wave station average terms. Blue represent fast arrivals and red represent slow arrivals. White stations have values between -0.1 and 0.1 (s). The symbol size represents the number of teleseismic earthquakes recorded by this station.

The map of differential travel time for S arrivals is shown in Figure 10. The values of  $\delta t$  range between -2.9 s and 3.8 s. Here, measurements were made for 615 events and 415 stations. The minimum number of events recorded by one station was 27 and the maximum was 441. In this map, it is possible to define four different regions with different patterns. The map of  $\delta t$  for SKS arrivals is shown in Figure 11. Here, the observed values of  $\delta t$  range between -3.1 s and 3.1 s. For this map, 510 events and 384 stations were used; the minimum number of events recorded by one station was 25 and the maximum was 234. Finally, we combined S and SKS arrivals into a single set of station averages (Figure 12). By combining these two types of phases we are obtaining arrivals from different incidence angles and are increasing the ray-path coverage. More than 615 events and 431 stations were used. The minimum number of events recorded by one station was 25 and the maximum was 497. Here, it is possible to observe values of  $\delta t$  that range between -2.9 s and 3.5 s from the array average and its distribution is shown in Figure 13.

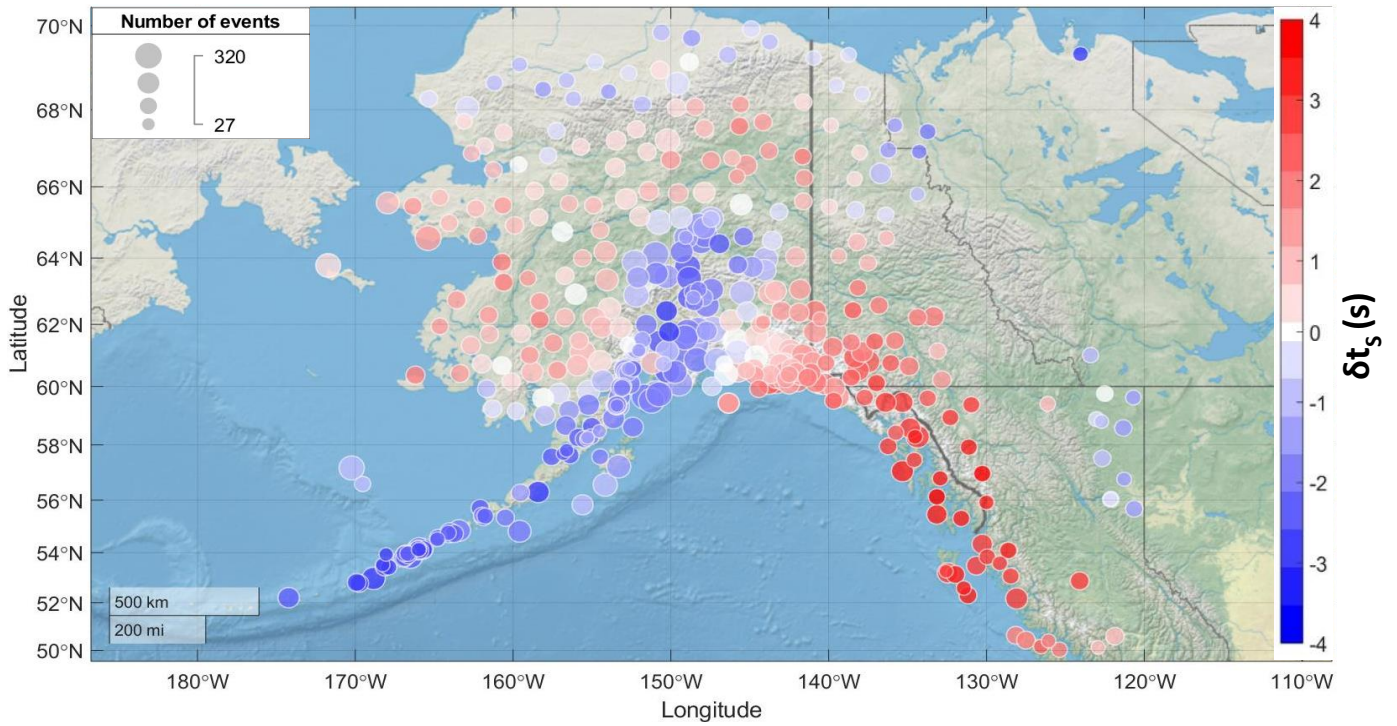


Figure 10:  $\delta t$  for S-wave station average terms. Blue represent fast arrivals and red represent slow arrivals. White stations have values between -0.1 and 0.1 (s). The symbol size represents the number of teleseismic earthquakes recorded by this station.

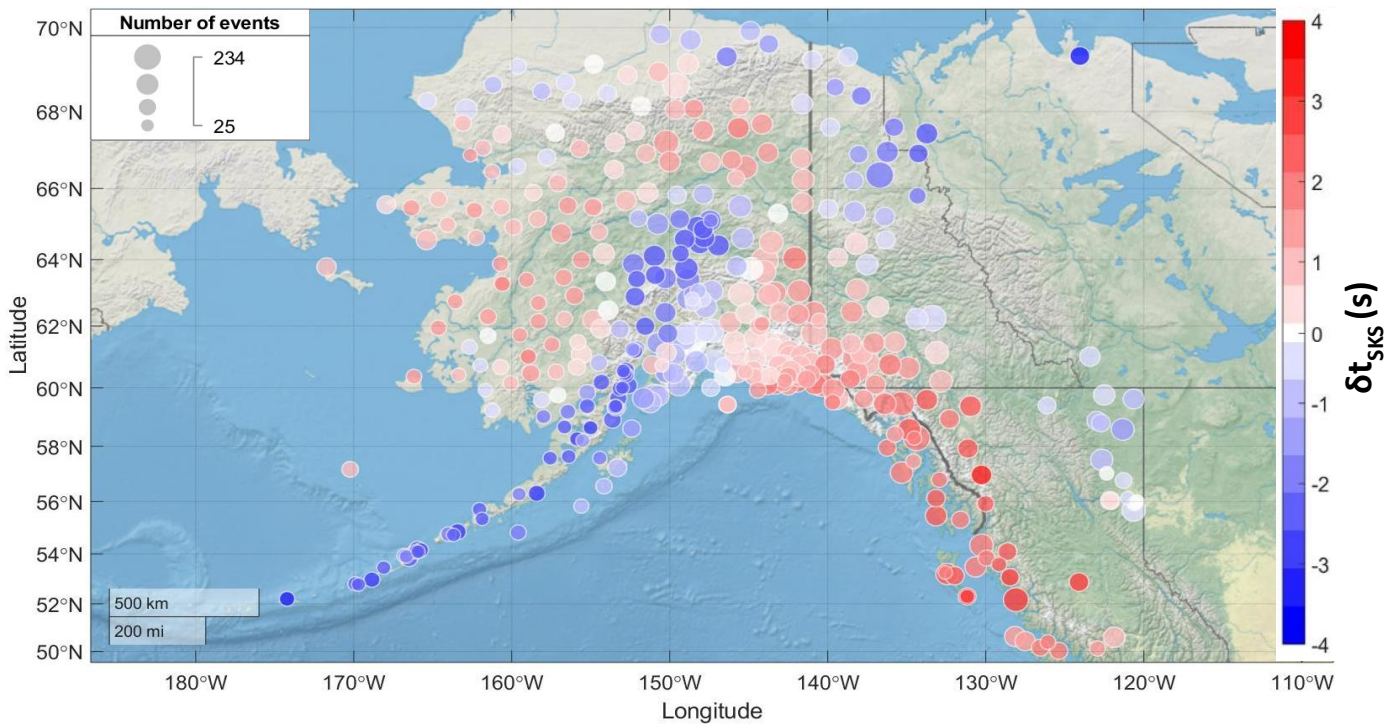


Figure 11:  $\delta t$  for SKS-wave station average terms. Blue represent fast arrivals and red represent slow arrivals. White stations have values between -0.1 and 0.1 (s). The symbol size represents the number of teleseismic earthquakes recorded by this station.

For these 3 maps, S, SKS and S-SKS as for the P arrivals, the first region that comprises the Aleutian arc show fast arrivals represented in blue. The second region comprises southeastern Alaska and northwestern Canada, this region shows some of the slowest arrivals in our study area, represented in red. The third region that comprises northernmost Alaska shows fast arrivals. The remaining area represents the fourth region and it shows moderately fast arrivals that are not present in the map of P-wave arrivals.

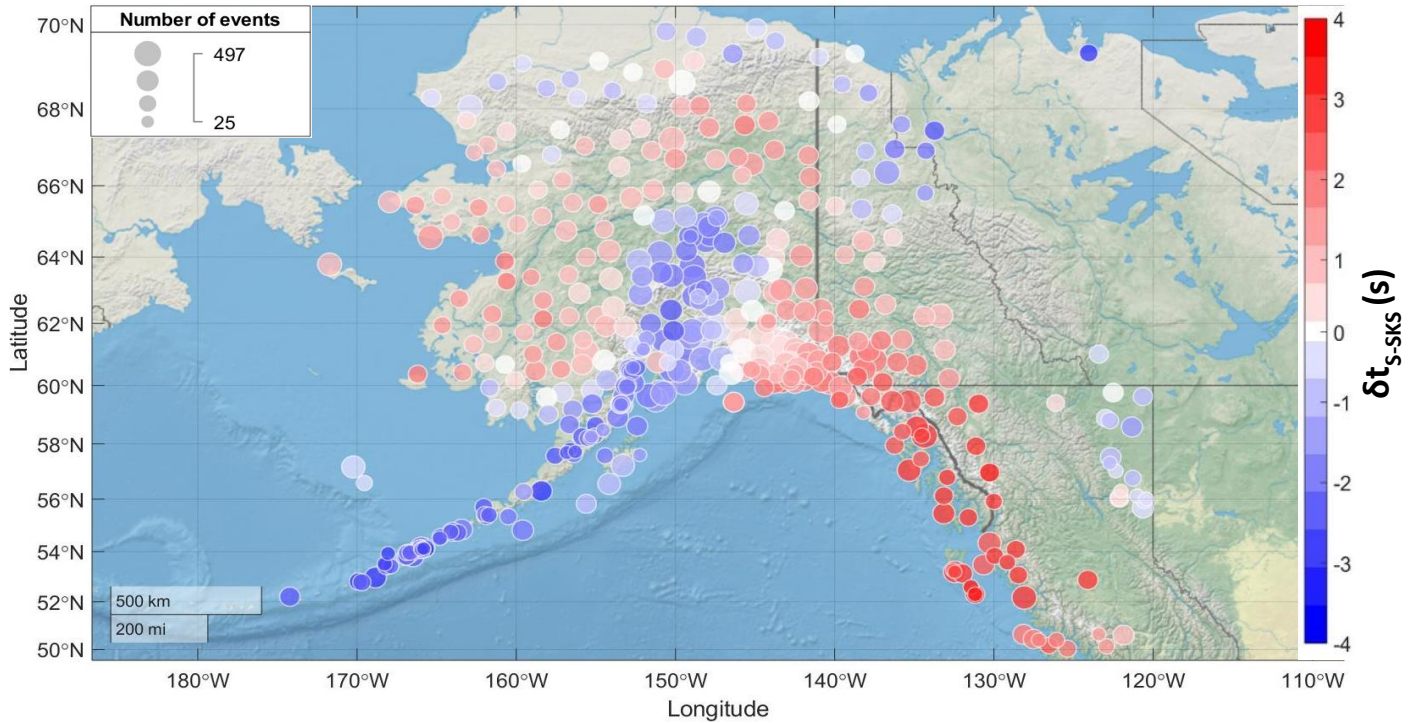


Figure 12:  $\delta t$  for S-wave and SKS-wave combined station average terms. Blue represent fast arrivals and red represent slow arrivals. White stations have values between -0.1 and 0.1 (s). The symbol size represents the number of teleseismic earthquakes recorded by this station.

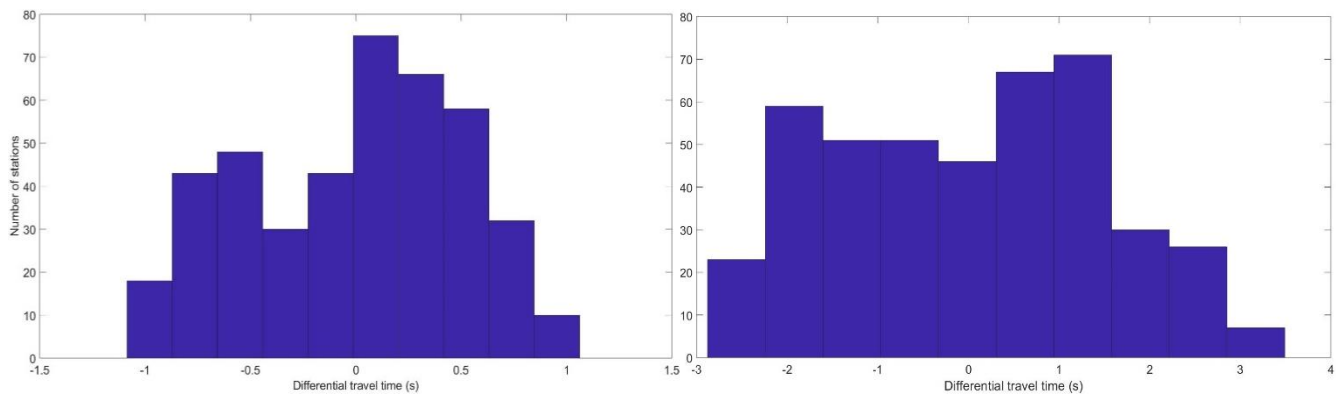


Figure 13: Histograms with the distribution of differential travel values averaged by station for A. P-wave arrivals. B. S-wave and SKS-wave combined.

## 5.2 Differential attenuation ( $\Delta t^*$ )

For this study we also calculated station averages for differential attenuation. In Figure 14, we show the  $\Delta t^*$  map for P arrivals. The values of  $\Delta t^*$  range between -1s and 0.6s. For this map, 634 events and 376 stations were used. The minimum number of events recorded by one station was 20 and the maximum was 252. In this map, more than half of the stations show values between -0.1s and 0.1s, approximately equal to the array average. Here, it is not possible to clearly observe the large-scale regions that we defined for the  $\delta t$  map of P arrivals since many of the stations have values close to the array average represented by white points. The rest of the stations represented with red and blue are consistent with the patterns identified previously.

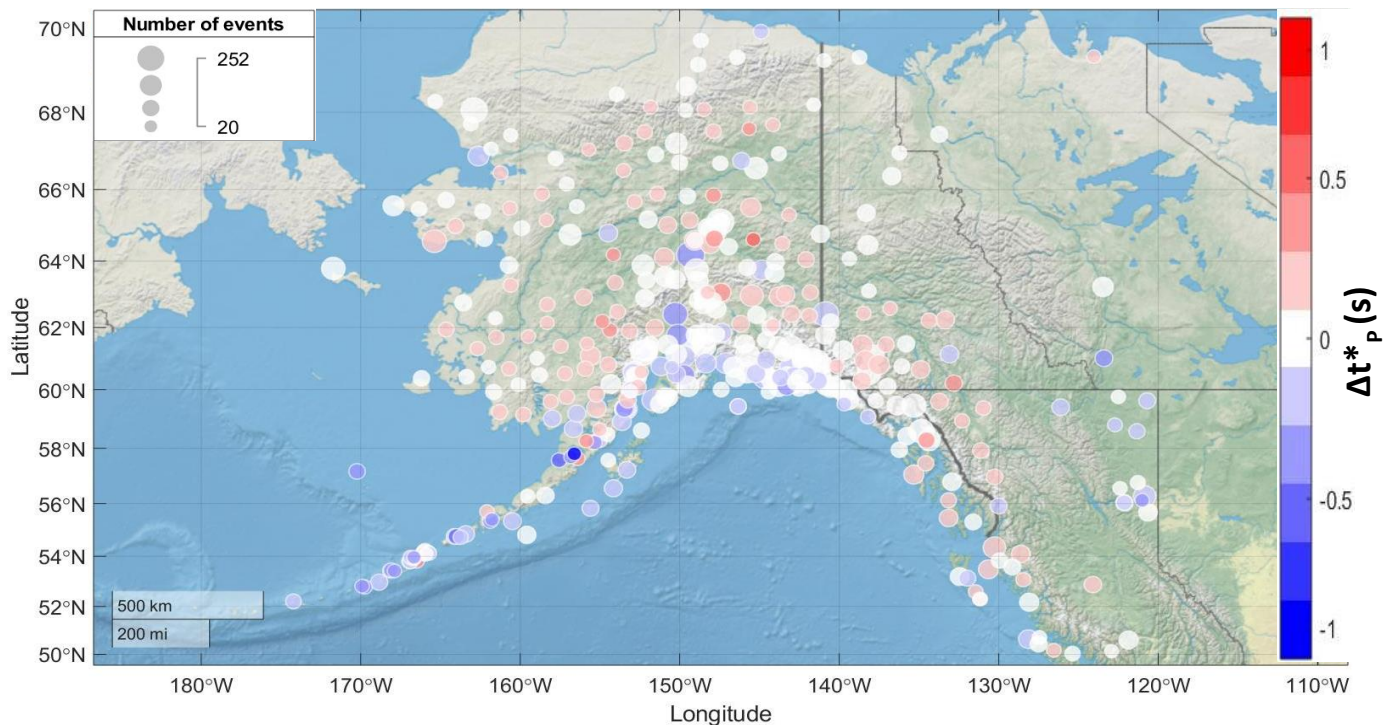


Figure 14:  $\Delta t^*$  for P-wave station average terms. White stations have values between -0.1 and 0.1 (s). The symbol size represents the number of teleseismic earthquakes recorded by this station.

We also calculated differential attenuation for S-wave (Figure 15), SKS-wave (Figure 16) and S-wave and SKS-wave combined (Figure 17) arrivals. The values of  $\Delta t^*$  for S arrivals range between -1.5s and 0.7s. For this map, 526 events and 413 stations were used, the minimum number of events recorded by one station was 20 and the maximum was 241. The observed values of  $\Delta t^*$  for SKS arrivals range between -1.1s and 0.8s. For this map, 408

events and 335 stations were used; the minimum number of events recorded by one station was 20 and the maximum was 194.

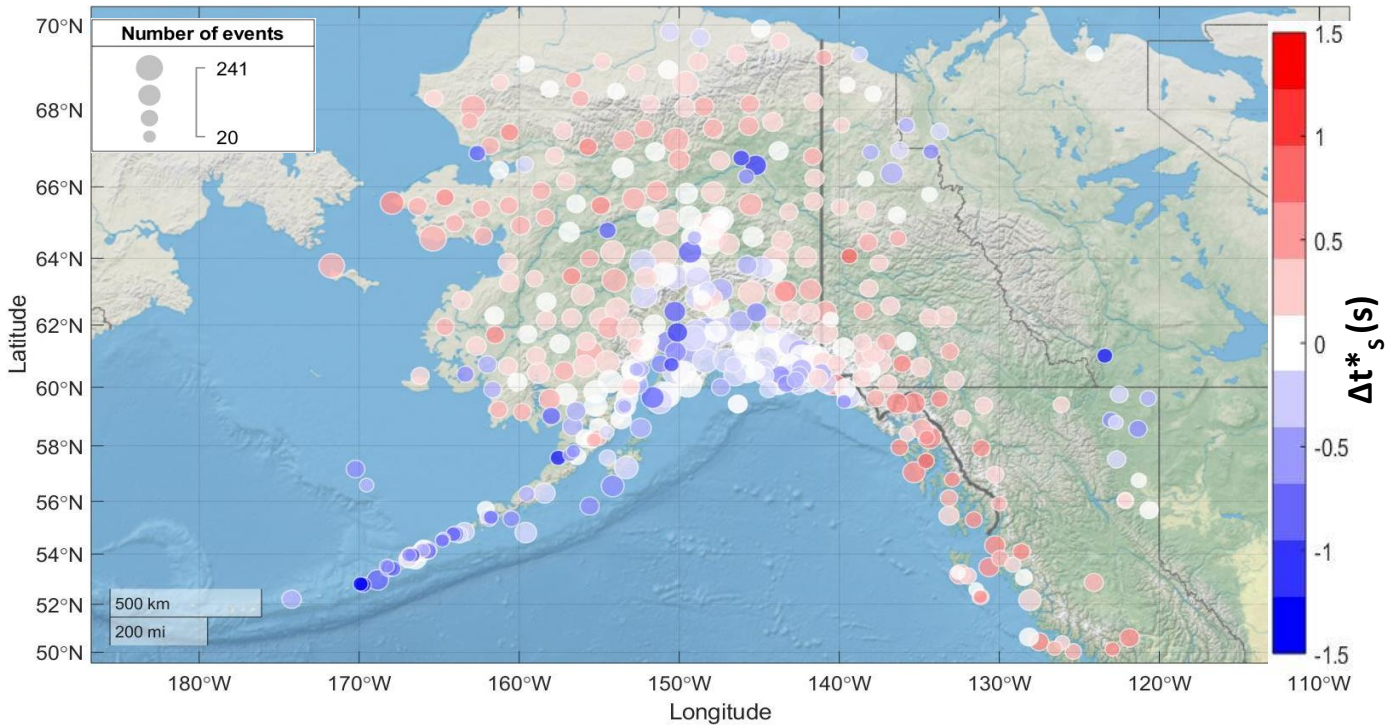


Figure 15:  $\Delta t^*$  for S-wave station average terms. White stations have values between  $-0.1$  and  $0.1$  (s). The symbol size represents the number of teleseismic earthquakes recorded by this station.

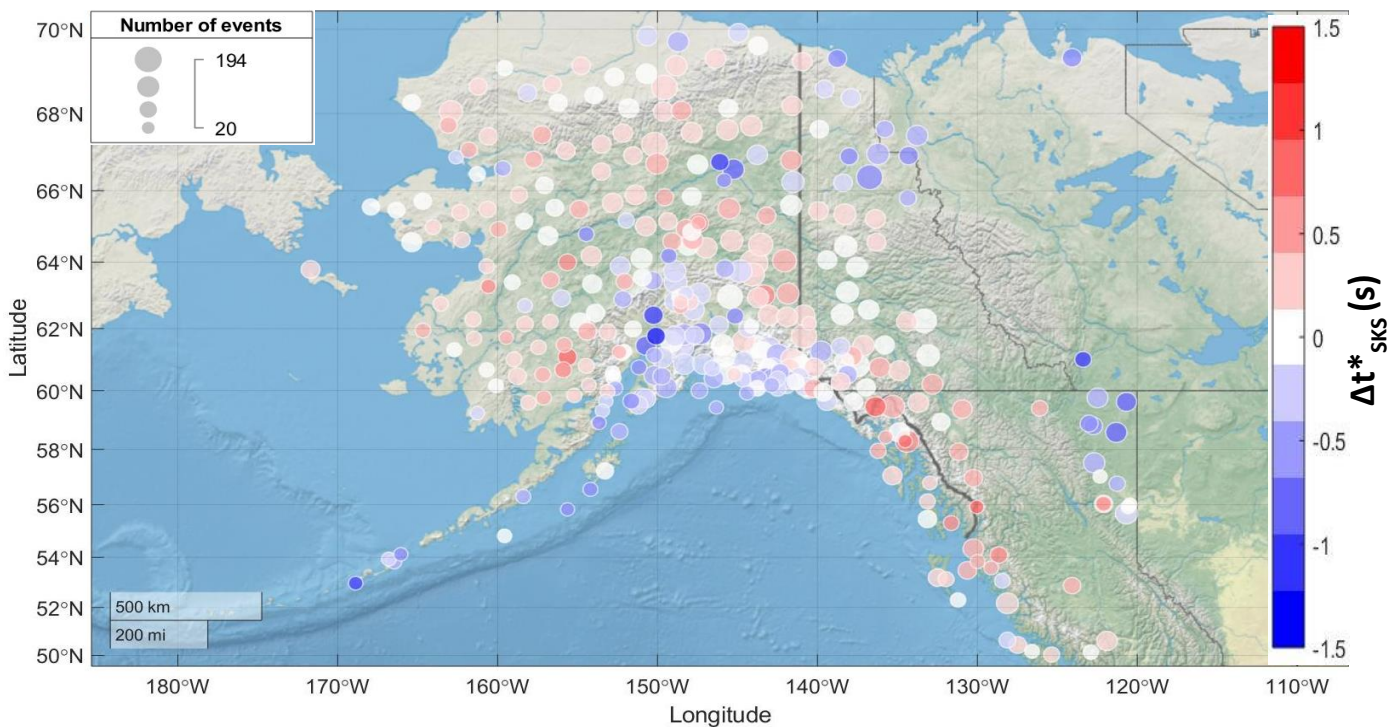


Figure 16:  $\Delta t^*$  for SKS-wave station average terms. White stations have values between  $-0.1$  and  $0.1$  (s). The symbol size represents the number of teleseismic earthquakes recorded by this station.

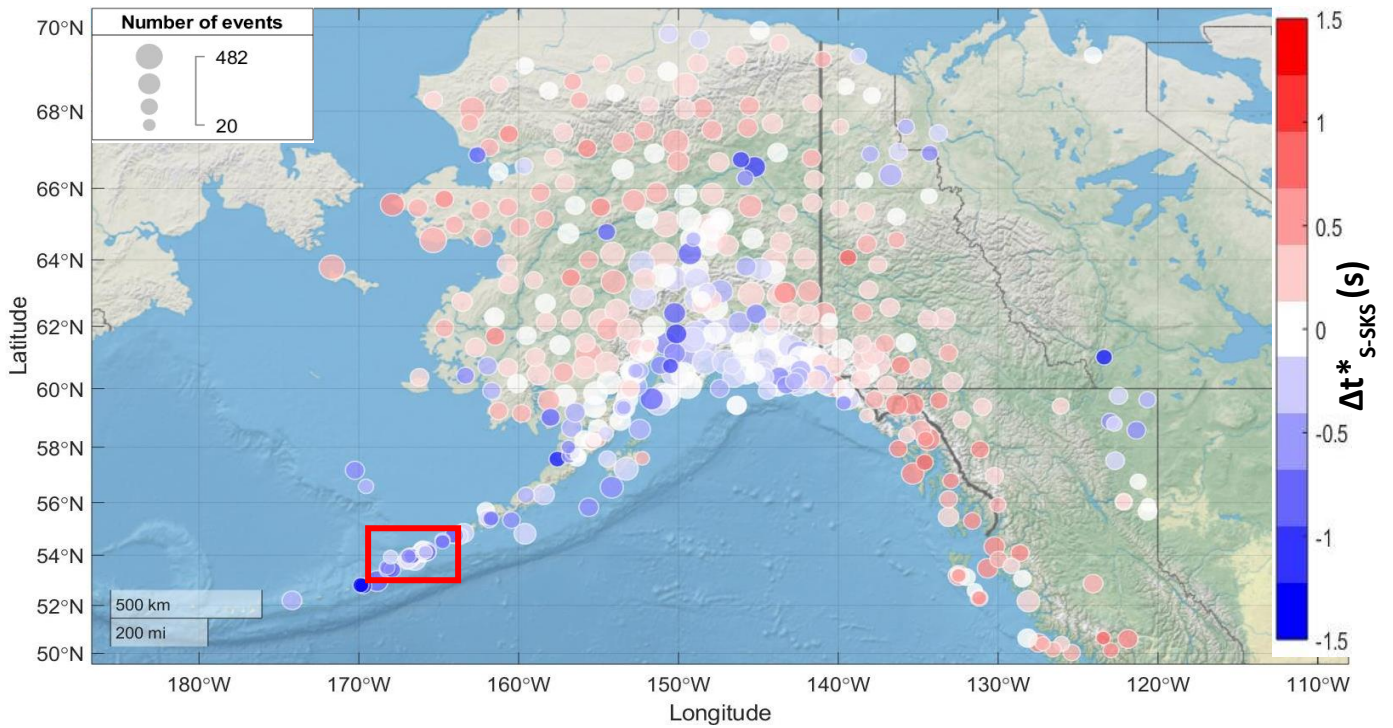


Figure 17:  $\Delta t^*$  for S-wave and SKS-wave combined station average terms. White stations have values between -0.1 and 0.1 (s). The symbol size represents the number of teleseismic earthquakes recorded by this station. The red rectangle represents the area of Figure 18.

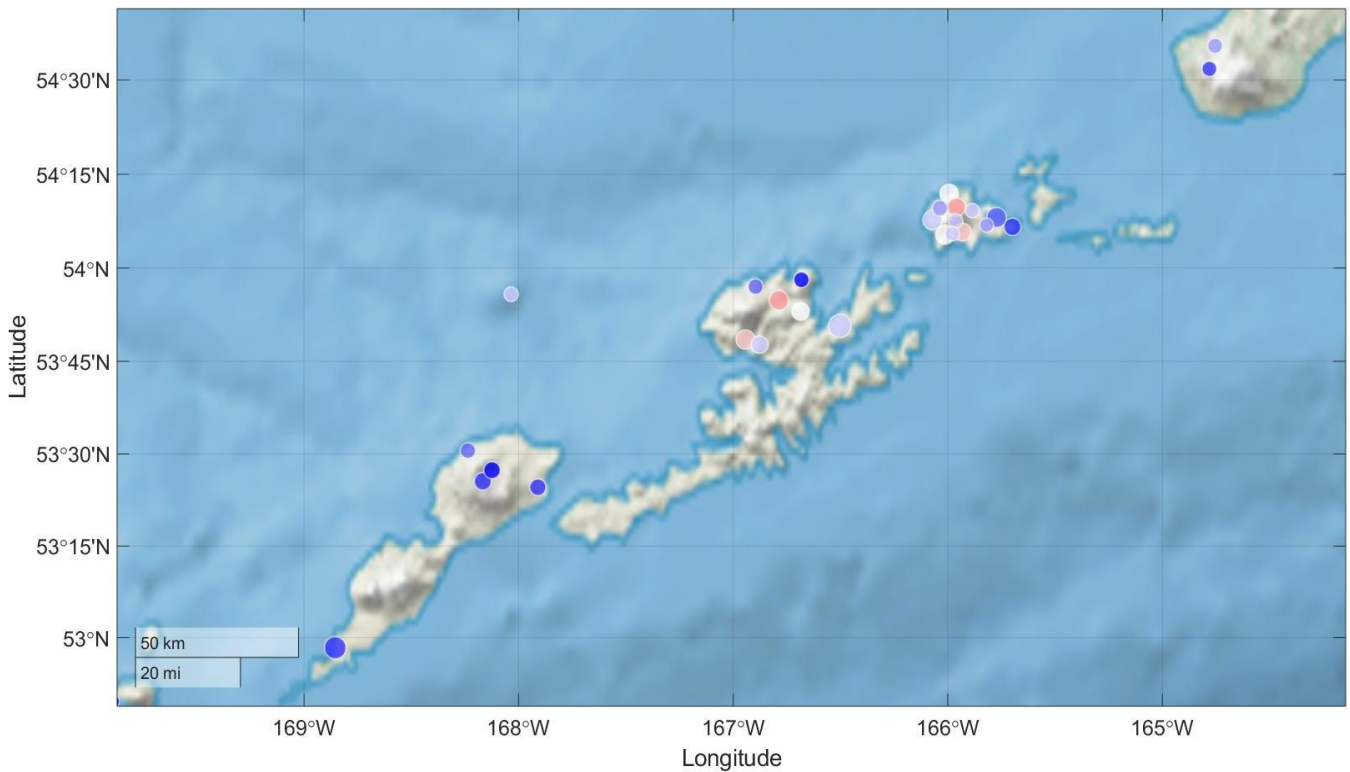


Figure 18:  $\Delta t^*$  for S-wave and SKS-wave combined station average terms. Zoom to a section of the Aleutian island arc. Location and color scale showed in Figure 17.

Finally,  $\Delta t^*$  values for S-SKS combined arrivals range between -1.5s and 0.7s (Figure 19). For this map, more than 526 events and 428 stations were used, the minimum number of events recorded by one station was 20, and the maximum was 252. These three maps have similar patterns in  $\Delta t^*$  and they are consistent with the maps of differential travel time except for a few specific regions that will be discussed in the next section.

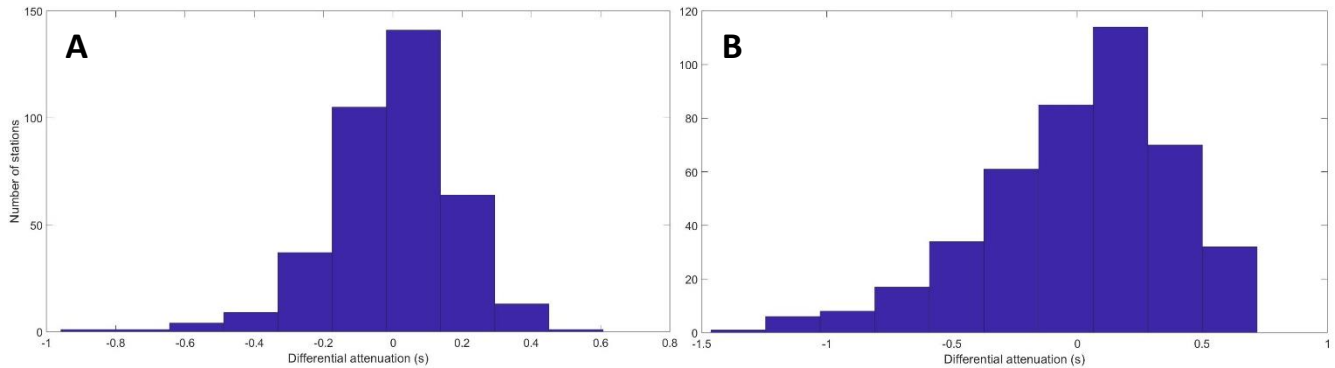


Figure 19: Histograms with the distribution of differential attenuation values station averaged for A. P-wave arrivals. B. S-wave and SKS-wave combined.

## 6. Discussion

Seismic travel times and attenuation can help us to elucidate the state of the Earth's interior. There are many factors that affect seismic attenuation and velocity in different ways. Among them are variations in rock properties such as temperature, melt content, composition, grain size, and seismic properties such as frequency. In general, attenuation increases as frequency increases; it means that higher frequencies will be attenuated more. Attenuation increases as temperature increases, and in the case of subduction zones, we can have relatively sharp temperature variations compared to other tectonic settings. Temperature can affect the density and the shear modulus of rocks and consequently, the velocity of seismic waves could be affected. Lower temperatures will increase the velocity and high temperatures will decrease velocity.

Water content promotes melting, and as the melt content increases attenuation will also increase. In the case of velocity as the melt content increases, velocity will decrease. Grain size has a different effect on attenuation, as grain size increases, attenuation decreases [Dalton and Faul, 2010].

Although these relationships have been clearly demonstrated in the lab, there are many competing effects that are not well understood [Abers et al., 2014]. For instance, a dry mineral will be stronger than a mineral that contains water; as the water content increases, the material is weakened, and attenuation should increase. However, high water content may also increase grain size, which will cause the contrary effect on attenuation [Dalton and Faul, 2010]. In many cases, temperature variations and water content are not enough to explain the values of attenuation. For example, attenuation is also dependent on the amount and mechanism of the melt transport, such as grain boundary sliding or melt squirt [Abers et al., 2014].

## 6.1 Tectonic interpretation

The large-scale variations in delay time and differential  $t^*$  can be interpreted in terms of the subduction of the Pacific plate beneath the North American Plate; the colder slab exhibits increased velocities and reduced attenuation relative to the array average. Adjacent areas show high attenuation and large delay times. The station averages contain information about a range of depths beneath each station. We defined several different regions using the spatially smoothed station averages for  $\delta t$  and  $\Delta t^*$  from S and SKS phases combined, which have the best resolution, to aid in the discussion (Figure 20).

Region A1 encompasses the Aleutian arc and is characterized by low attenuation and high velocities. It is highly coherent in  $\delta t$  and we interpret this to be due to arrivals with a significant portion of the ray path through the subducting slab. In this region, there is more variability in attenuation than in delay time. While most stations have relatively low values of attenuation, some stations do not follow the general pattern of the area and show high values of attenuation (Figure 18). We can interpret these very localized variations as the result of local melting associated with the active volcanoes present in this area. Specifically, in Figure 18 we can observe that the eastern region with high attenuation values coincides with the Akutan volcano that is one of the most active volcanoes of the Aleutian arc. Its last eruption occurred in 1992 [Alaska Volcano Observatory]. The other region with high

attenuation values coincides with Makushin volcano that erupted in 1995 [Miller et al., 1998].

Region A2 comprises central-western Alaska. This area shows moderately high values of attenuation and moderately low values of velocity. We interpret this to be the result of waves traveling primarily through the mantle wedge, which is expected to be relatively low velocity and high attenuation, but with some contribution to the ray path from the subducting slab, for earthquakes to the southeast of the study area. This contribution is clearly demonstrated in Figure 21A, which shows individual measurements of  $\delta t$  for P-wave arrivals arranged by back azimuth. In Figure 21B we can observe that the back azimuthal patterns in attenuation are not as clear as the patterns for velocity.

Region A3 is a region with a similar pattern as A2 but here the values of  $\delta t$  and  $\Delta t^*$  are higher. This area comprises southeastern Alaska and western Canada and the low values of velocity and high values of attenuation are expected since this is an active margin.

A4 is a zone with early arrivals for S and SKS phases in northern Alaska; this pattern is not clear for the P arrivals and for attenuation maps since they show slow arrivals for P-wave and high attenuation for all the phases. This pattern can also be observed in mid-ocean ridges where melt content affects more velocity than attenuation. Based on their velocity maps, this area was interpreted by Jiang et al. (2018) as cold strong lithosphere that is guiding the intraplate deformation. There is a signature of melt but most likely it is not present in this area. And according to our observations given that we obtained fast velocities and moderate values of attenuation, it can be explained by a melt-depleted composition area.

We also defined region A5 which comprises the Yakutat plate area, where we can observe late arrivals but low attenuation values. This can be interpreted in terms of the important amount of sediments that are being subducted in this area or the active volcanism the Wrangell volcanic field that is believed to be the result of a slab tear that allows hot asthenosphere to upwell [Wech, 2016]. Finally, the easternmost stations are in a region we

define as region A6. It shows low values of attenuation and high values of velocities which we interpret as a region of thicker continental lithosphere and although it is in the limit of the deformation, it is older and thicker continental lithosphere.

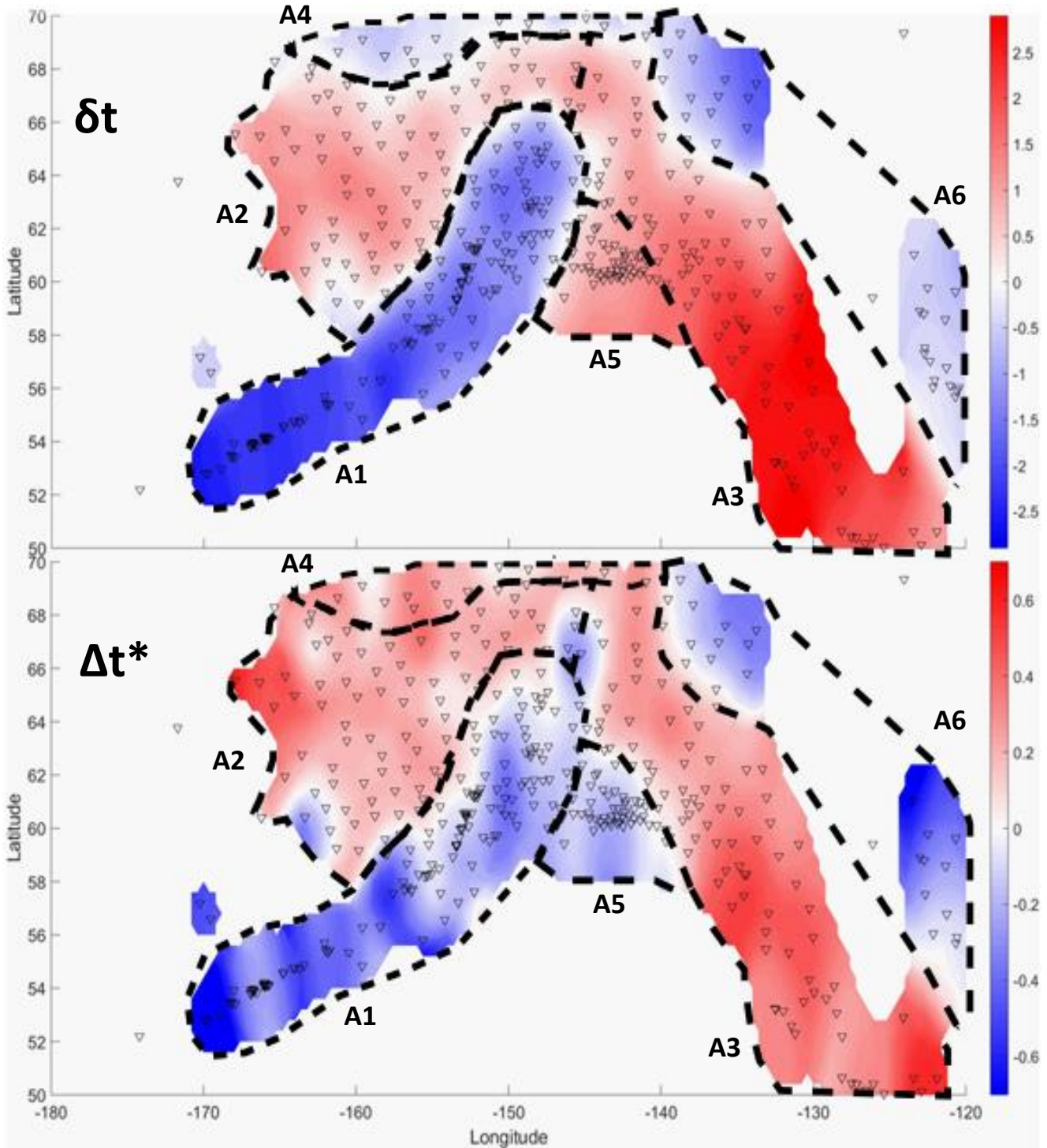


Figure 20: Smoothed maps of A.  $\Delta t$  B.  $\Delta t^*$  for S-wave and SKS-wave combined. Interpreted regions are labeled from A1 to A6.

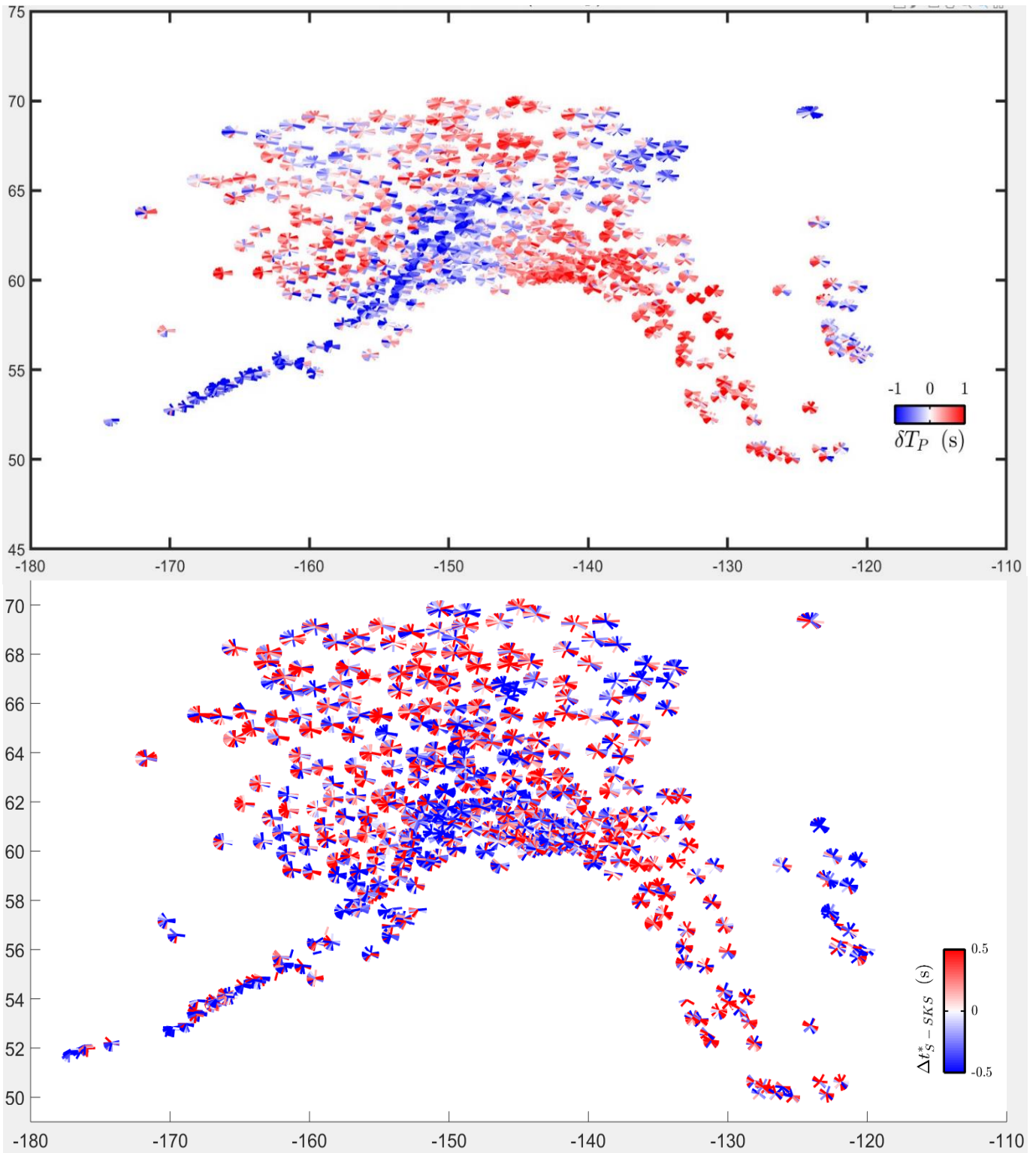


Figure 21: Individual measurements as function of back-azimuth for every event for A.  $\delta t$  P-wave and B.  $\Delta t^*$  S-wave and SKS-wave combined.

## 6.2 Uncertainty

It is important to consider all the possible sources of uncertainty that could be introduced at many stages during this study. Measurements of arrivals assume a smooth ray path, but this is not always the case. Scattering is a crucial factor to consider in this type of study since it can be an important source of uncertainty specially in continental studies. There is more scattering in continental crust than in oceanic crust where we expect a more homogeneous material [Eilon and Abers, 2017]. Scattering can cause us to over or underestimate the values of attenuation in a non-systematic way. The station average we carry out is an attempt to reduce the effect of scattering and focus on the attenuation values. Additionally, we smooth these maps to minimize the uncertainty created by scattering and focus on the attenuation of large-scale patterns.

Another different source of uncertainty is related to the sources of the teleseismic events. The least-square problem used to obtain our station averages is formulated in a way in which these uncertainties are very small. Since these results are differential measurements none of the data are sensitive to the absolute attenuation, or any attenuation close to the source that is commonly recorded across all receivers. Moreover, there are different types of analysis that could be applied in order to reduce any remaining source effects. For instance, Lawrence et al. (2006) used cluster analysis to map attenuation beneath North America. This analysis allows to associate different quadrants based on waveforms; in this way, it is possible to reduce the source effects. However, instead of applying this method, we achieve a similar result by rejecting measurements with poor correlation.

Different sources of uncertainty could also be associated with the processing of the data. The cross-correlation process could give us an important source of uncertainty, and a decent rule of thumb is that the measurement uncertainties are about  $1/20$  of the dominant period at which the signals were filtered [Vandercar and Crosson, 1990]. In addition, while measuring differential attenuation we are applying many calculations such as the calculation of the spectrum or the least square regression, and these calculations can have several errors as well.

Finally, since our array does not present a systematic distribution of stations, it is possible to have uncertainty that comes from the station spacing. There are some areas with high station coverage while there are other areas where there are not many stations. This non-systematic distribution could increase the uncertainty not only for the smoothed maps but also for the future tomographic inversions.

## 7. Conclusions

We have elucidated the attenuation and velocity patterns beneath Alaska and western Canada using teleseismic body-waves: P, S and SKS, obtained from the DMC of IRIS. After the processing of our data we obtained the best available attenuation maps of Alaska to date. These maps allowed us to interpret the large-scale geophysical structures of Alaska. Our results show the presence of six regions with different velocity and attenuation patterns within our study area. First, the region that comprises the Aleutian volcanic arc. Two regions have the same patterns in  $\delta t$  and  $\Delta t^*$  but different magnitudes on their measurement: one region comprises central-western Alaska and the other comprises southeastern Alaska and western Canada. We can distinguish regions at northernmost Alaska and the Yakutat plate. And finally, some of the easternmost stations of the study area are on the limit of deformation and closer to stable continental values. Each area presents different large-scale patterns in attenuation, velocity or both compared to the other.

## 8. Future work and recommendations

The results of this study provide an important framework for understanding the large-scale geophysical structures of Alaska. However, our final maps average across internal 3-D heterogeneity. For this reason, as future work, we will tomographically invert our  $\delta t$  and  $\Delta t^*$  measurements for 3D structure using a finite frequency approach. The results of this inversion process will help us to understand better the distribution of the velocity and attenuation anomalies beneath Alaska. We also strongly recommend continuing working on

this research by calculating the absolute values of attenuation. Finally, we wish to highlight that there is a lot of free access data from this area and it could be used in order to produce other studies of this type.

## Bibliography

- Abers, G. A., Fischer, K. M., Hirth, G., Wiens, D. A., Plank, T., Holtzman, B. K., ... and Gazel, E. (2014). Reconciling mantle attenuation-temperature relationships from seismology, petrology, and laboratory measurements. *Geochemistry, Geophysics, Geosystems*, 15(9), 3521-3542.
- Anderson, D. L., and Hart, R. S. (1976). An earth model based on free oscillations and body waves. *Journal of Geophysical Research*, 81(8), 1461-1475.
- Bauer, M. A., Pavlis, G. L., and Landes, M. (2014). Subduction geometry of the Yakutat terrane, southeastern Alaska. *Geosphere*, 10(6), 1161-1176.
- Beikman, H. M. (1980). Geologic Map of Alaska, US Geol. *Survey Special Map. scale, 1(2,500)*.
- Benz, H.M., Dart, R.L., Villaseñor, Antonio, Hayes, G.P., Tarr, A.C., Furlong, K.P., and Rhea, Susan, 2011, Seismicity of the Earth 1900–2010 Aleutian arc and vicinity: U.S. Geological Survey Open-File Report 2010–1083-B, scale 1:5,000,000.
- Bianco, F., Castellano, M., Del Pezzo, E., and Ibanez, J. M. (1999). Attenuation of short-period seismic waves at Mt Vesuvius, Italy. *Geophysical Journal International*, 138(1), 67-76.
- Brown, J. R., Prejean, S. G., Beroza, G. C., Gomberg, J. S., and Haeussler, P. J. (2013). Deep low-frequency earthquakes in tectonic tremor along the Alaska-Aleutian subduction zone. *Journal of Geophysical Research: solid earth*, 118(3), 1079-1090.
- Bruns, T. R. (1983). Model for the origin of the Yakutat block, an accreting terrane in the northern Gulf of Alaska. *Geology*, 11(12), 718-721.
- Byrne, T. (1979). Late Paleocene demise of the Kula-Pacific spreading center. *Geology*, 7(7), 341-344.
- Cafferky, S., and Schmandt, B. (2015). Teleseismic P wave spectra from USArray and implications for upper mantle attenuation and scattering. *Geochemistry, Geophysics, Geosystems*, 16(10), 3343-3361.
- Christeson, G. L., Gulick, S. P., van Avendonk, H. J., Worthington, L. L., Reece, R. S., and Pavlis, T. L. (2010). The Yakutat terrane: Dramatic change in crustal thickness across the Transition fault, Alaska. *Geology*, 38(10), 895-898.
- Coats, R. R. (1962). Magma type and crustal structure in the Aleutian arc. *The crust of the Pacific Basin*, 6, 92-109.

- Coulson, S., Garth, T., and Rietbrock, A. (2018). Velocity structure of the subducted Yakutat terrane, Alaska: Insights from guided waves. *Geophysical Research Letters*, *45*(8), 3420-3428.
- Dalton, C. A., and Ekström, G. (2006). Global models of surface wave attenuation. *Journal of Geophysical Research: Solid Earth*, *111*(B5).
- Dalton, C. A., Ekström, G., and Dziewoński, A. M. (2008). The global attenuation structure of the upper mantle. *Journal of Geophysical Research: Solid Earth*, *113*(B9).
- Dalton, C. A., and Faul, U. H. (2010). The oceanic and cratonic upper mantle: Clues from joint interpretation of global velocity and attenuation models. *Lithos*, *120*(1-2), 160-172.
- Eilon, Z. C., and Abers, G. A. (2017). High seismic attenuation at a mid-ocean ridge reveals the distribution of deep melt. *Science advances*, *3*(5), e1602829.
- Fee, D., Haney, M. M., Matoza, R. S., Van Eaton, A. R., Cervelli, P., Schneider, D. J., and Iezzi, A. M. (2017). Volcanic tremor and plume height hysteresis from Pavlof Volcano, Alaska. *Science*, *355*(6320), 45-48.
- Gudmundsson, O., Finlayson, D. M., Itikarai, I., Nishimura, Y., and Johnson, W. R. (2004). Seismic attenuation at Rabaul volcano, Papua new Guinea. *Journal of volcanology and geothermal research*, *130*(1-2), 77-92.
- Gung, Y., and Romanowicz, B. (2004). Q tomography of the upper mantle using three-component long-period waveforms. *Geophysical Journal International*, *157*(2), 813-830.
- Havskov, J., and Alguacil, G. (2004). *Instrumentation in earthquake seismology* (Vol. 358). Dordrecht, The Netherlands: Springer.
- Jiang, C., Schmandt, B., Ward, K. M., Lin, F. C., and Worthington, L. L. (2018). Upper Mantle Seismic Structure of Alaska From Rayleigh and S Wave Tomography. *Geophysical Research Letters*, *45*(19), 10-350.
- Karato, S. I., and Jung, H. (1998). Water, partial melting and the origin of the seismic low velocity and high attenuation zone in the upper mantle. *Earth and Planetary Science Letters*, *157*(3-4), 193-207.
- Karato, S. I., and Spetzler, H. A. (1990). Defect microdynamics in minerals and solid-state mechanisms of seismic wave attenuation and velocity dispersion in the mantle. *Reviews of Geophysics*, *28*(4), 399-421.
- Koons, P. O., Hooks, B. P., Pavlis, T., Upton, P., and Barker, A. D. (2010). Three-dimensional mechanics of Yakutat convergence in the southern Alaskan plate corner. *Tectonics*, *29*(4).

- Lawrence, J. F., Shearer, P. M., and Masters, G. (2006). Mapping attenuation beneath North America using waveform cross-correlation and cluster analysis. *Geophysical research letters*, 33(7).
- Margerin, L. (2011). Seismic waves, scattering. *Encyclopedia of Solid Earth Geophysics*, 1210-1223.
- Miller, T. P., McGimsey, R. G., Richter, D. H., Riehle, J. R., Nye, C. J., Yount, M. E., and Dumoulin, J. A., 1998, Catalog of the historically active volcanoes of Alaska: U.S. Geological Survey Open-File Report 98-0582, 104 p.
- McNamara, D. E., and Pasyanos, M. E. (2002). Seismological evidence for a sub-volcanic arc mantle wedge beneath the Denali volcanic gap, Alaska. *Geophysical Research Letters*, 29(16), 61-1.
- Müller, R. D., Sdrolias, M., Gaina, C., and Roest, W. R. (2008). Age, spreading rates, and spreading asymmetry of the world's ocean crust. *Geochemistry, Geophysics, Geosystems*, 9(4).
- Piccinini, D., Di Bona, M., Lucente, F. P., Levin, V., and Park, J. (2010). Seismic attenuation and mantle wedge temperature in the northern Apennines subduction zone (Italy) from teleseismic body wave spectra. *Journal of Geophysical Research: Solid Earth*, 115(B9).
- Plafker, G., Moore, J. C., Winkler, G. R., and Berg, H. C. (1994). Geology of the southern Alaska margin. *The geology of Alaska*, 1.
- Reid, F. J. L., Woodhouse, J. H., and Van Heijst, H. J. (2001). Upper mantle attenuation and velocity structure from measurements of differential S phases. *Geophysical Journal International*, 145(3), 615-630.
- Romanowicz, B. (1995). A global tomographic model of shear attenuation in the upper mantle. *Journal of Geophysical Research: Solid Earth*, 100(B7), 12375-12394.
- Roth, Erich G., et al. "Seismic attenuation tomography of the Tonga-Fiji region using phase pair methods." *Journal of Geophysical Research: Solid Earth* 104.B3 (1999): 4795-4809.
- Ruppert, N. A., Lees, J. M., Kozyreva, N. P., and Eichelberger, J. (2007). Seismicity, earthquakes and structure along the Alaska-Aleutian and Kamchatka-Kurile subduction zones: A review. *GEOPHYSICAL MONOGRAPH-AMERICAN GEOPHYSICAL UNION*, 172, 129.
- Scholl, D. W., Vallier, T. L., and Stevenson, A. J., 1987, Geologic evolution and petroleum geology of the Aleutian Ridge, in Scholl, D. W., Grantz, A., and Vedder, J. G., eds., Geology and resource potential of the continental margin of western North America and adjacent ocean basins—Beaufort Sea to Baja California: Houston, Texas, Circumpacific Council for Energy and Mineral Resources, p. 123–155.

Selby, N. D., and Woodhouse, J. H. (2002). The Q structure of the upper mantle: Constraints from Rayleigh wave amplitudes. *Journal of Geophysical Research: Solid Earth*, 107(B5), ESE-5.

Shearer, P. M. (2009). *Introduction to seismology*. Cambridge University Press.

Shito, A., Karato, S. I., Matsukage, K. N., and Nishihara, Y. (2006). Towards mapping the three-dimensional distribution of water in the upper mantle from velocity and attenuation tomography. *GEOPHYSICAL MONOGRAPH-AMERICAN GEOPHYSICAL UNION*, 168, 225.

Stachnik, J. C., Abers, G. A., and Christensen, D. H. (2004). Seismic attenuation and mantle wedge temperatures in the Alaska subduction zone. *Journal of Geophysical Research: Solid Earth*, 109(B10).

Stein, Seth, and Michael Wyssession. *An introduction to seismology, earthquakes, and earth structure*. John Wiley and Sons, 2009.

Steven Holbrook, W., Lizarralde, D., McGeary, S., Bangs, N., and Diebold, J. (1999). Structure and composition of the Aleutian island arc and implications for continental crustal growth. *Geology*, 27(1), 31-34.

Teng, T. L. (1968). Attenuation of body waves and the Q structure of the mantle. *Journal of Geophysical Research*, 73(6), 2195-2208.

Thomson, D. J. (1982). Spectrum estimation and harmonic analysis. *Proceedings of the IEEE*, 70(9), 1055-1096.

Wang, Y., and Tape, C. (2014). Seismic velocity structure and anisotropy of the Alaska subduction zone based on surface wave tomography. *Journal of Geophysical Research: Solid Earth*, 119(12), 8845-8865.

Wech, A. G. (2016). Extending Alaska's plate boundary: Tectonic tremor generated by Yakutat subduction. *Geology*, 44(7), 587-590.

## Web resources

Alaska Volcano Observatory. Retrieved from:

<https://avo.alaska.edu/>

Earthquake distribution of Alaska. Retrieved from:

<https://earthquake.alaska.edu/>

Transportable Array Deployment to Alaska and Western Canada. Retrieved from:

<http://www.usarray.org/alaska>

Transportable Array Deployment to Alaska and Western Canada. Retrieved from:

<http://ds.iris.edu/ds/>